INL/JOU-21-65465-Revision-0

Sensitivity and Reliability of Key Electrochemical Markers for Detecting Lithium Plating during Extreme Fast Charging

February 2022

Tanvir R Tanim, Eric J Dufek, Charles C Dickerson, Meng Li, Parameswara R. Chinnam

Changing the World's Energy Future

INL is a U.S. Department of Energy National Laboratory operated by Battelle Energy Alliance, LLC

INL/JOU-21-65465-Revision-0

Sensitivity and Reliability of Key Electrochemical Markers for Detecting Lithium Plating during Extreme Fast Charging

Tanvir R Tanim, Eric J Dufek, Charles C Dickerson, Meng Li, Parameswara R. Chinnam

February 2022

Idaho National Laboratory
Idaho Falls, Idaho 83415

http://www.inl.gov

Prepared for the
U.S. Department of Energy
Under DOE Idaho Operations Office
Contract DE-AC07-05ID14517

Sensitivity and Reliability of Key Electrochemical Markers for Detecting Lithium Plating during Extreme Fast Charging

Parameswara R. Chinnam[1], Tanvir R. Tanim[2,*], Eric J. Dufek[2] , Charles C. Dickerson[2] and Meng Li[2]

[1] Previous INL employee and currently at Rivian

[2] Energy Storage & Advanced Transportation Department, Idaho National Laboratory, Idaho Falls, ID 83415

[*]Corresponding author

KEYWORDS: Lithium-ion battery, Extreme fast charging, Electrochemical Li plating, Battery safety

ABSTRACT

Lithium plating is one of the key challenges for enabling extreme fast charging (XFC, ≤10 to 15 min charging at ≥6C) in graphite-based lithium-ion batteries. Significant R&D effort has been focused on how to mitigate Li plating. Parallel effort is also being devoted to developing methods to detect Li plating when and if it happens during fast charging. In that regard, electrochemical (EC) signature-based detection techniques are less resource intensive, more convenient, and more practical from an end-user application perspective. However, a comprehensive understanding of key plating related EC signatures for extreme fast charging is presently unavailable. In particular, there exist distinct issues of unreliability with key plating-related EC signatures—e.g., incremental capacity ($dQ.dV^{-1}$), differential OCV ($dOCV.dt^{-1}$), end of lithiation (EOL) rest voltage—at XFC conditions, and the underlying reasons have not been explored and identified methodically. Using a comprehensive test matrix and XFC conditions with Li/graphite half cells, this article highlights the unreliability issues associated with the EC Li plating diagnostics and explains the underlying root cause. This study finds distinct sensitivity and unreliability issues with plating related $dQ.dV^{-1}$, $dOCV.dt^{-1}$, and EOL rest voltage signatures with charging rates. The complex interaction between graphite and plated Li that happens through multiple competing mechanisms —Li stripping and chemical intercalation— at different charging rates is at the core of the sensitivity and unreliability issue.

INTRODUCTION

Limited driving range and long charging time for lithium-ion battery (LiB) electric vehicles (EVs), compared with internal combustion engine vehicles, cause "range anxiety" that inhibits their widespread adoption [1]. Extreme fast charging (XFC, ≤10 to 15 min charging at ≥6C) can narrow the gap between refueling and recharging [2]; therefore, it holds the potential for offering similar experiences at the gas or charging station, eliminating the barrier of adoption. However, during XFC batteries are prone to lithium (Li) plating, potentially creating catastrophic life and safety consequences [3-8]. These limitations have led the research and development (R&D) community devote significant efforts to better understand and develop means to detect Li plating using myriad methods and tools [8]. Many of the highlighted methods in Ref [8]. are *ex situ*—i.e., not suitable for *operando* detection. They aim to provide a comprehensive understanding of Li plating mechanisms and how those mechanisms impact LiB performance, life, and safety. Among various Li-plating detection methods that exist in the literature, with different scope and complexities [10], *operando* electrochemical (EC) lithium-detection techniques are convenient and practical diagnostics for on-board applications. EC methods of Li detection primarily rely on two mechanisms that occur after plating on graphite-based LiBs: (i) chemical intercalation (CI) of plated Li into graphite and (ii) stripping of the reversible component of plated Li from the graphite surface [6, 8]. These two mechanisms and associated EC signatures vary distinctly based on cell design, operating temperature, charging rate, rest time after charging, discharge rate after charging, etc., and as such often introduce unreliability in detection [6, 9-15]. Moreover, cell aging could further introduce additional ambiguity in electrochemical detection of Li plating. These factors, combinedly, have created confusion on the reliability and applicability of EC Li-plating signatures for XFC conditions.

The most widely used EC Li plating detection metrics include coulombic efficiency (CE), incremental capacity (IC or $dQ.dV^{-1}$), differential voltage (DV or $dV.dQ^{-1}$), differential open-circuit voltage ($dOCV.dt^{-1}$), end-of-charge voltage (EOCV) tracking, and impedance [4-7, 9, 11, 13, 15-18]. Some of these metrics have been shown to have stable and reliable performance for sub-zero temperatures [11-13, 16, 19] or skewed negative: positive-electrode ratio cells (N:P<1) [18]. However, those same metrics have distinct sensitivity and unreliability issues for XFC conditions, which is typically implemented at or above room temperatures [7-9, 13, 20]. For instance, a distinct IC or DV signature can be obtained at subzero temperatures [11, 13, 21-23], but at higher temperatures, those very signatures show ambiguity [8, 9]. Having a constant voltage step or rest

during or after charging also introduces unreliability in EC detection of Li plating at temperatures higher than ambient [9]. Kim et al. and Anseán et al. observed plating relevant IC signatures in skewed N:P ratio cells (by design or due to aging) even at non-XFC conditions [4, 18] whereas Chen et al. recently concluded that IC signature associated with Li plating is unreliable for XFC conditions up to 9C [8]. Another recent study by Konz et al. on Li/graphite half cells concluded that $dOCV.dt^{-1}$ is a reliable EC signature for moderate charging rates up to 4C [7]; however, Chen et al.'s study on single layer gr/NMC pouch cells up to 6C found $dOCV.dt^{-1}$ to be an unreliable detection signature for Li-plating [8]. The $dOCV.dt^{-1}$ signature in Chen's research momentarily shows up during cycling for very aggressive plating conditions, but quickly vanishes afterwards [8]. Others have also reported similar unreliability issues with $dOCV.dt^{-1}$ at 30°C [5, 14, 24]. The discussion thus far with conflicting messages highlights the confusion the R&D community and the diagnostics end-users have on the broad reliability of EC Li-plating detection signatures and their applicability for XFC conditions.

Therefore, a distinct need exists to clarify the highlighted confusions on the sensitivity and reliability of EC Li-plating signatures for XFC conditions, along with root causes. Through a comprehensive test matrix, this study leveraging electrochemistry provides clarity on the elusive behavior of the EC detection of Li plating and explains the root cause of unreliability. The test matrix executed in this study includes different EC Li detection signatures for various plating scenarios and cycling conditions—e.g., 1C to 6C with state-of-charge (SOC) variation between 20 and 110%, with and without rest, and with aging. A key aspect of using just electrochemical methods in the current study is that they are among the most directly applicable methods for on-board diagnostics.

MATERIALS AND METHODS

Materials. All experiments were performed with 170 μm thick, 1.42 cm^2 Li and 1.27 cm^2 graphite (Li/graphite) in CR2032 coin cells. The graphite electrode prepared at Cell Analysis, Modeling and Prototyping (CAMP) Facility, Argonne National Laboratory, consists of 91.83 wt% Superior Graphite SLC 1506T, 2 wt% Timcal C45 carbon, 6 wt% Kureha 9300 PVDF binder, 0.17 wt% oxalic acid on 10 μm thick Cu foil with a total coating thickness of 70 μm, 38.2% porosity, and ~3.0 $mAhcm^{-2}$ capacity based on formation at C/10 cycling. The same anode has been used in multiple other studied in full pouch cells for the eXtreme Fast Charge Cell Evaluation of Lithium-ion Batteries (XCEL) Program [3, 25, 26].

Cell Preparation. Punched electrodes were dried overnight in a vacuum at 80°C. Celgard 2320, with 1.58 cm^2 used as a separator after drying overnight in vacuum. 28 µL (~6× pore volume of anode and separator) 1.2 M $LiPF_6$ in 3:7 EC:EMC (by weight) was used as the electrolyte; all electrolyte components were purchased from BASF. During cell preparation, 14 µL electrolyte was placed on Li metal before placing separator and another 14 µL on separator before placing graphite electrode. After assembly, the cells were maintained at a temperature of 25 ±1°C in an environmentally controlled chamber (TestEquity 1007C). A MACCOR 4000 Series Automated Test System was used for all electrochemical evaluations. Scanning electron microscopy (SEM) was performed with a JEOL JSM 6610LV instrument. SEM samples were prepared in an argon-filled glovebox and had minimal exposure to ambient: only during transfer of the specimens to the SEM chamber.

Electrochemical Evaluation. Upon cell build, the cells were placed in an environmental chamber and equilibrated for 2.5 h before applying three formation cycles: C/10 (0.4 mA) charge-discharge between 1.5 and 0.005 V, with one-hour rest in between. Each cell then underwent a single beginning-of-life (BOL) C/20 charge and discharge cycle within 1.5–0.005 V at the current determined by the last C/10 discharge capacity during formation. The BOL discharge capacity is taken as 100% capacity for SOC calculation and used to scale variable SOC conditions or extent of lithiation as well.

After formation and BOL testing, 25 cells were grouped into 11 subgroups, as shown in Table 1. Each group had triplicate or duplicate of cells, encompassing different C-rate and SOC (lithiation) test conditions with and without rest, as discussed in Table 1. The detailed electrochemical tests for each group are listed in Table T1 in SI. Plating was induced by applying either 10% overlithiaiton (OL) for 1C rate or a high rate charging—i.e., 3C to 6C, up to 60% SOC.

Coulombic efficiency (CE), which accounts for the loss of Li, was calculated by dividing delithiation (discharge) capacity over lithiation (charge) capacity for a particular cycle. The stripping efficiency (SE) is the ratio of reversible Li to the total amount of plated Li, $Q_{rev.plating}/(Q_{rev.plating} + Q_{irrev.plating})$, where $Q_{rev.plating} = Q_{stripping}$, $Q_{irrev.plating} = Q_{ch} - Q_{dis}$, and Q_{ch} = lithiation (charge) capacity and Q_{dis} = delithiation (discharge) capacity. Discharge capacity below 0.09 V (<0.1 V, the first deintercalation potential for gr) is considered as $Q_{rev.plating}$ [9]. Lithium stripping and deintercalation from graphite surface are competing processes during discharge at high voltages, but Li stripping favors over

deintercalation because of its lower standard electrode potential than graphite deintercalation that typically starts at or above ~0.1V. Therefore, stripping plateau appears before 0.1V, graphite deintercalation plateau and is wider for increased amounts of stripped Li [18, 19].

Table 1: Experimental test matrix. All discharge (or delithiation) was performed at C/5 after reaching the desired SOC.

Group	**Test condition**	**EC signature**
A (3)	6C charge (lithiation) to 20% SOC, followed by up to 60% SOC with 5% increment. Cycling at the same rate at 60% SOC (alternate with rest and no rest after charge)	Effect of SOC on $dQ.dV^{-1}$, and $dOCV.dt^{-1}$ signatures
B (3)	6C charge to 40% SOC, followed by up to 40% SOC with 5% increment. Cycling at the same rate at 40% SOC (alternate with rest and no rest after charge)	Effect of SOC on $dQ.dV^{-1}$, and $dOCV.dt^{-1}$ signatures
C (2)	6C charge to 60% SOC. No rest after charge.	$dQ.dV^{-1}$ sensitivity and reliability at 6C (60% SOC)
D (2)	6C charge to 60% SOC. 30 min rest after charge.	$dOCV.dt^{-1}$ sensitivity and reliability at 6C (60% SOC)
E (2)	6C charge to 40% SOC. No rest after charge.	$dQ.dV^{-1}$ sensitivity and reliability at 6C (40% SOC)
F (2)	6C charge to 40% SOC. 30 min rest after charge	$dOCV.dt^{-1}$ sensitivity and reliability at 6C (40% SOC)
G (2)	1C charge to 110% SOC. No rest after charge.	$dQ.dV^{-1}$ sensitivity and reliability at 1C (110% SOC)
H (3)	1C charge to 110% SOC. No rest after charge. Long-term testing	Long-term $dQ.dV^{-1}$ sensitivity and reliability at 1C (110% SOC)
I (2)	3C charge to 60% SOC. 30 minutes rest after charge.	$dOCV.dt^{-1}$ sensitivity and reliability at 3C (60% SOC)
J (2)	3C charge to 60% SOC. No rest after charge.	$dQ.dV^{-1}$ sensitivity and reliability at 3C (60% SOC)
K (2)	1C charge to 110% SOC. 30 min rest after charge *Long-term testing	Long-term $dOCV.dt^{-1}$ sensitivity and reliability at 1C (110% SOC)

RESULTS AND DISCUSSION

Effect of charging rate on electrochemical plating detection signatures. Figure 1 presents early cycling data to exhibit the sensitivity of charging rate (1C to 6C) and extents of lithiation (up to 110% SOC) to relevant EC Li-plating signatures (Groups C, E, G, and J)—namely, CE, SE, and dQ.dV-1. Figures S1 and S2 present the cycle-by-cycle voltage versus lithiated- and delithiated-capacity plots for the same conditions for additional clarity. CE and SEs are interdependent, and provide information on the extent of irreversibility, and reversibility, respectively, of the Li, whereas a dQ.dV-1 stripping peak below Stage I graphite intercalation potential (~0.1 V) provides additional confirmation that Li plating has already occurred. The conditions highlighted in Figure 1 have no rest after lithiation (or charge) minimizing chemical intercalation (CI) of plated Li into graphite, hence providing the best possible scenario for capturing Li stripping mechanism through SE and $dQ.dV^{-1}$ metrics.

Both CE and SE suffer with increased charge rate, as displayed in Figure 1A. The decrease in CE with increased C-rate indicates more irreversible loss of Li at the anode during charge or lithiation. Closer examination of the highest C-rate conditions—i.e., 6C—reveals the presence of distinct polarization shortly after charging began, driving the cell voltage well below 0 V (see Figures S1, S2 and S3) in the Li-plating regime. The higher polarization associated with higher rate can primarily be attributed to electrolyte-transport limitation across the anode, which eventually depletes the Li^+ from the electrolyte, yielding highly nonuniform impedance and graphite use [25, 26]. The extent of polarization would create conditions for simultaneous intercalation and plating, where plating reaction dominates over intercalation [27]. Concurrently, the plated Li will chemically intercalate into the graphite [11]. This simultaneous CI with plating during charge leaves less Li for later stripping, resulting in lower SE in Figure 1A at 6C. The higher anode polarization will also enhance the electrolyte reduction at the anode, causing more irreversible consumption of Li and/or plated Li (hence, the lower CE and SE), that would have otherwise available for stripping (Figure 1A).

Plating at aggressive charging rates, but to a greater extent of SOC, has weak impact on the reversibility behavior of Li, as shown in the comparative plots between 6C-40% SOC and 6C-60% SOC cases in Figure 1A. To obtain more clarity on the effects of SOC on Li reversibility, we tested additional conditions (Group A in Table1 and Table S1), where cells were charged at 6C from 20 to 60% SOC, in 5% increments for each cycle without any rest after charge. The results are shown in

Figures S4, S5A, S5C, and S5E. Charging to higher SOC extends the plating regime that would favor more Li plating and irreversible loss of Li, visible through reduced CE in Figure S5A. Simultaneously, the increase in $dQ.dV^{-1}$ peak intensity or stage length, in Figs. S4B, S4D, S5C and S5E, during discharge with SOC indicate more graphite utilization, primarily due to concurrent chemical intercalation during lithiation. Therefore, increased irreversible Li loss together with chemical intercalation, combinedly, contributed to very weak SE (Figures 1A and S5A), which plateaus only around 20%, irrespective of SOCs when charging rate remains very high, i.e., 6C. Relaxing the C-rate to 3C and charging up to the same SOC level (i.e., 60%) in Figure 1A shows distinct improvements in reversibility (i.e., higher CE and SE) than 6C conditions. These observations confirm that fast-charging rate has a stronger impact on Li reversibility than SOC (or SOC threshold) for XFC conditions.

Figure 1A shows that plating at lower C-rate, i.e., 1C, has even better reversibility behavior of Li than the higher C-rate conditions. In particular, the 1C plating condition has distinctly higher CE and SE (~4× higher) than 6C conditions. Unlike 6C case, cells at 1C experience less polarization, particularly towards the end of charge due overlithiation (Figure S1A), thereby driving less Li plating and simultaneous CI of plated Li during charge. The less-polarized state will also favor less electrolyte decomposition, consuming less Li irreversibly. Besides these two factors, fast-charge-driven rapid exhaustion of electrolyte in the anode has previously been tied to predominantly dendritic lithium formation, whereas low- or moderate-rate plating is primarily linked to mossy Li formation [25, 29–31]. Dendritic lithium converts to dead lithium (loss of electrical contact with graphite, covered by thicker SEI) more quickly due to its having larger surface area and higher reactivity with the electrolyte. Mossy-lithium morphology (surface area, etc.), on the other hand, is homogenous and has lower reactivity with the electrolyte [12, 32]. Thus, dendritic Li has shown lower reversibility than mossy Li [23]. This leads to the conclusion that distinctly different plated-Li morphology at the 1C rate is another factor affecting the extent of reversibility observed in Figure 1A. We note that the higher polarization and preferential Li plating at 3C and 6C, which creates a high competition between intercalation of plated Li and Li stripping, make the SE comparison less comparable to 1C-110% SOC.

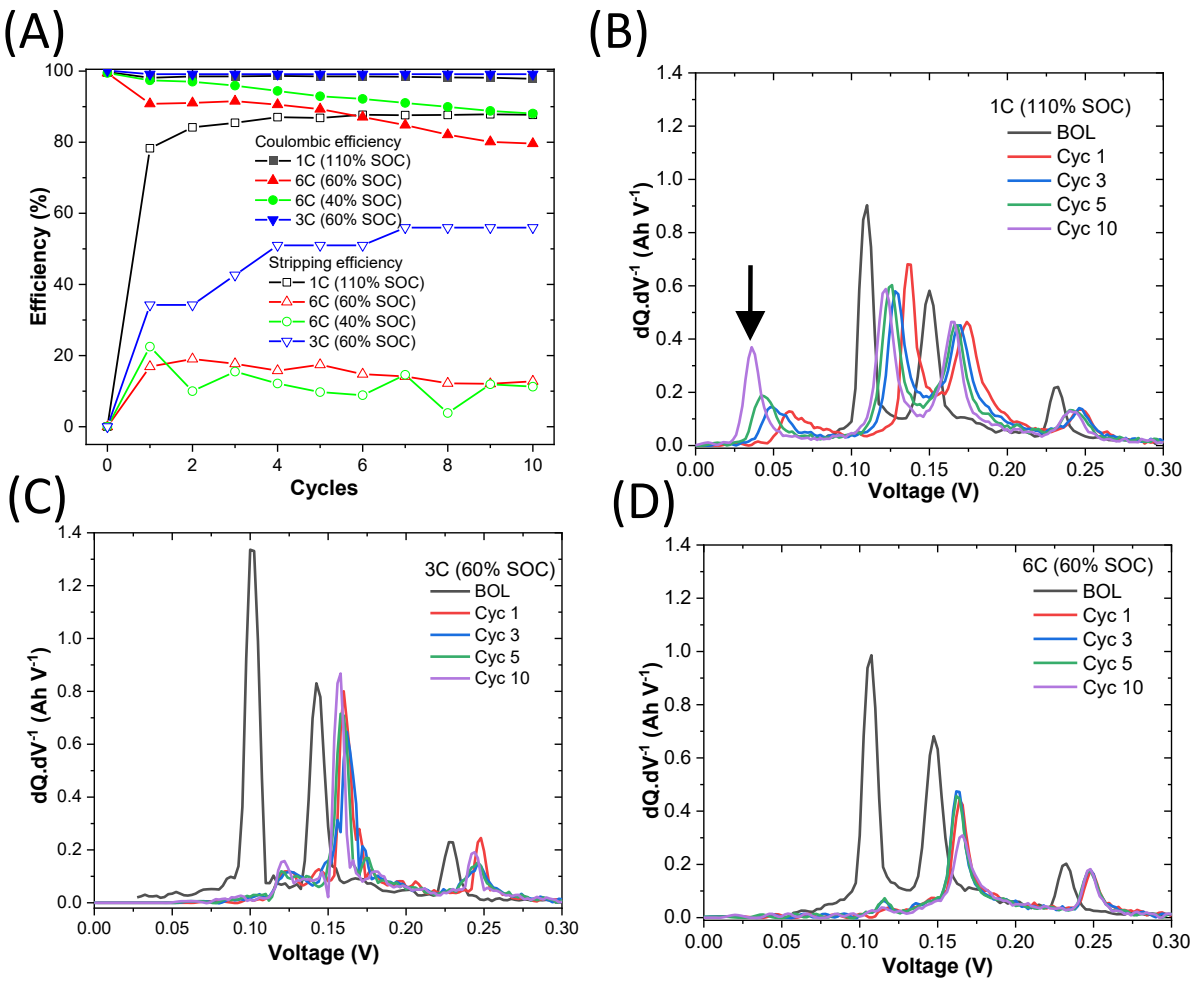

Figure 1. A) Comparison of CE and lithium SE for Li/graphite half-cells at 1C charge up to 110% SOC, 3C charge up to 60% SOC, 6C charge 60% SOC and 40% SOC followed by C/5 discharge with no rest. B) C/5 discharge dQ.dV^{-1} curves after 1C charge 110% SOC with no rest. The arrow points Li stripping peak below 0.1V. C) Discharge dQ.dV^{-1} curves after 3C charge 60% SOC with no rest. D) Discharge dQ.dV^{-1} curves after 6C charge 60% SOC with no rest. Note that one cell data from each group is shown at each cycling condition.

The reversibility behavior of plated Li has left clear imprints on the relevant dQ.dV^{-1} curves presented in Figures 1B–D and Figure S5 (showing the 6C different SOC conditions). No dQ.dV^{-1} signature (below 0.1V) associated with Li stripping is observed for the 6C case, irrespective of SOC throughout cycling up to 10 (Figures 1C and D), both of which had less than 20% SE (Figure 1A). The 3C-60% case, despite having medium SE (between 50 and 60%, Figure 1A), did not produce any noticeable dQ.dV^{-1} signature either associated with Li stripping within Cycle 10 (Figure 1C). Distinct dQ.dV^{-1} signature is only visible for the 1C-110% SOC condition from the very beginning

(Figure 1B, below 0.1 V identified by the arrow) having ≥80% SE. Upon cycling, the SE slightly increases up to 85% at Cycle 10 and the $dQ.dV^{-1}$ peak associated with Li stripping strengthens while shifting gradually towards Li/Li+ equilibrium potential. Moreover, the $dQ.dV^{-1}$ peaks change in size and shape with cycling, which could be an indication of uneven stripping and/or kinetics due to surface irregularities [28]. The increased SE (Figure 1A) and the relevant $dQ.dV^{-1}$ stripping signature (Figure 1B) for 1C charging rate could primarily be attributed to distinctly higher reversible capacity of plated Li, as shown in Figures S6 and S7, as compared to the higher C-rate conditions.

In summary, we conclude that $dQ.dV^{-1}$ is an unreliable signature to detect Li plating for XFC conditions. Multiple reasons contribute to this unreliability during XFC condition. First, a significant portion of the plated Li becomes irreversible due to converting to more electrically isolated Li (or dead Li) and reacting with electrolyte at higher polarization. Secondly, simultaneous CI during lithiation that depletes the reversible part of plated Li. These mechanisms combinedly depletes enough reversible fraction of plated Li to suppress the $dQ.dV^{-1}$ (or $dV.dQ^{-1}$) stripping signature, a key diagnostic for Li plating widely accepted in other plating conditions—e.g., low temperature, low N:P ratio, etc. Tanim et al. [3, 9] and Chen et al., [8] in their recent XFC studies evaluated fast charging between 4C to 9C up to ~97% SOC in full cells with different cell loadings using the same graphite material. They did not find any evidence of Li stripping related $dQ.dV^{-1}$ signature even though other signs of plating were evident. The experimental observations and the derived insights presented thus far support those full-cell observations, pinpoint the underlying reasons, and confirm that $dQ.dV^{-1}$ is an unreliable Li-plating detection diagnostic for XFC conditions.

Long-term Li reversibility, $dQ.dV^{-1}$ sensitivity and reliability. Next, we examine the long-term reversibility behavior of plated Li and the relevant signatures for the 1C-110% SOC condition that showed distinct and stable plating signatures in early cycles. Shown in Figure 2A, the rate of CE decrease remains moderate up to ~10 cycles, which then accelerates until the cell failed at 29th cycle. In line with Figure 2A trends, Figure 2D shows comparable irreversible capacity loss with cycling. The SE, on the other hand, stays above 80% up to 10 cycles, then decreases rapidly, primarily due to increased amount of irreversible loss as shown in Figure 2D. The absolute values of stripped Li, however, increase consistently until ~25 cycles (Figure 2D) due to more and more available plated Li for stripping that consequently contributes to stronger Li stripping $dQ.dV^{-1}$ signatures in Figure 2B. The increased Li stripping with cycling could primarily be attributed to

more Li plating that compensated for less graphite utilization. Figures 2B and 2C both show a gradual reduction in graphite stage I–III peak intensities during discharge and charge, respectively, that can be directly attributed to less graphite utilization as cycling progressed. This decrease in graphite utilization could be caused by blocked intercalation pathways (reduced porosity), loss of active material, localized electrolyte dry out, etc. [29, 30]. Towards later cycling (around Cycle 25), the graphite peaks completely disappear, and the stripping peak becomes most dominant, essentially indicating the cell turned from Li/gr to Li-Li symmetric cell. Closer examination of Figure 2B also reveals that the dQ.dV^{-1} shoulder related to Li stripping, indicated by the arrow, gradually take different shape with cycling, an indication that all the Li may not have stripped uniformly, which may be due to kinetic differences between stripping associated with surface irregularities [28].

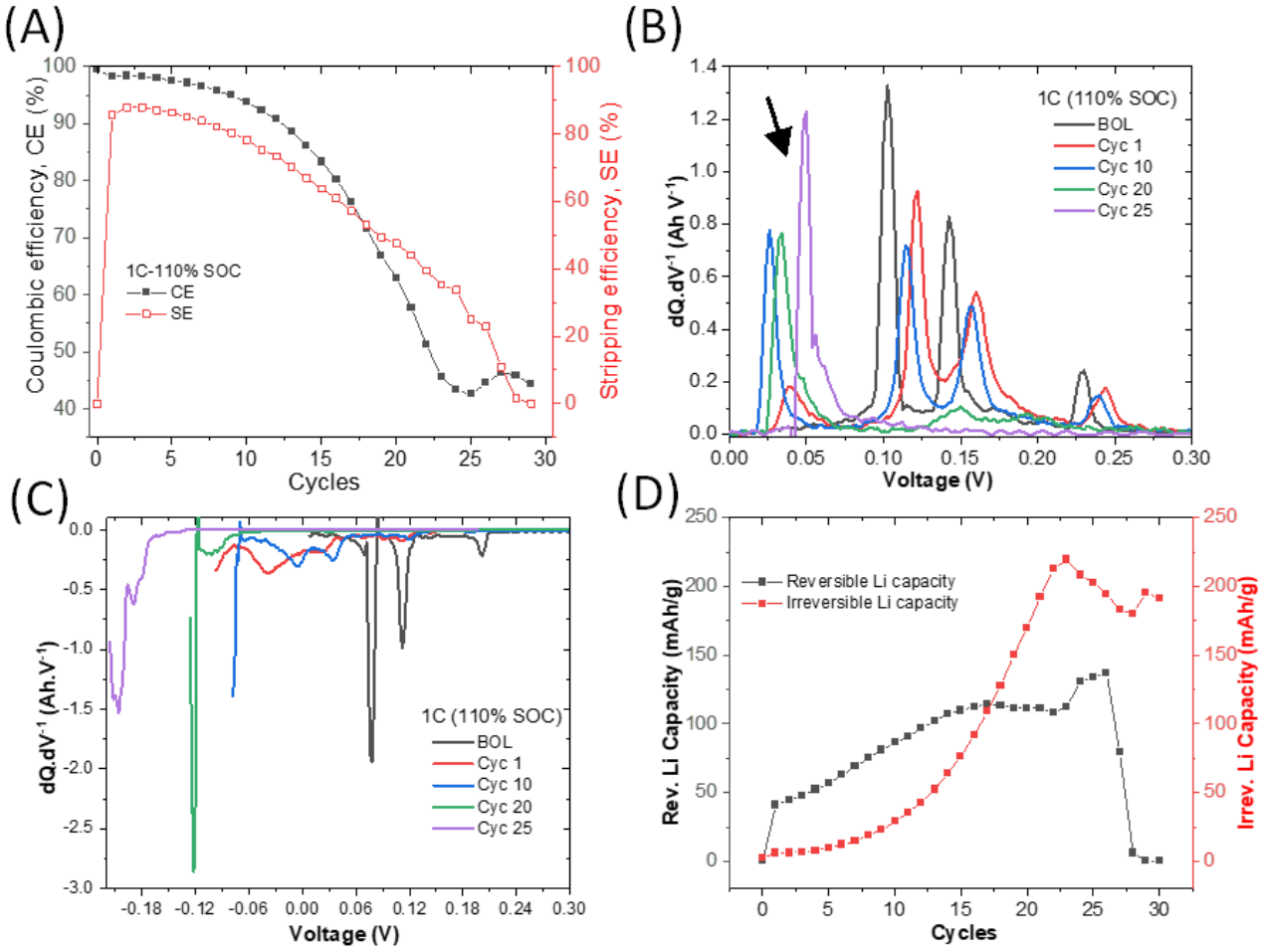

Figure 2. A) Long-term coulombic and lithium stripping efficiency for Li/graphite half-cells at 1C charge 110% SOC with no rest followed by C/5 discharge. B) C/5 discharge dQ.dV^{-1}

curves after 1C charge 110% SOC with no rest. The arrow points Li stripping peak below 0.1V. C) 1C charge dQ.dV^{-1} curves to 110% SOC. D) Reversible and irreversible Li capacities at 1C charge 110% SOC with no rest followed by C/5 discharge.

Sensitivity and Reliability of dOCV.dt^{-1}. The dOCV.dt^{-1} plateau, identified by an arrow in Figure 3, results from CI of electrically connected Li upon plating on graphite [6]. Here we explore the sensitivity of dOCV.dt^{-1} plateau for different XFC conditions—e.g., 6C charge up to either 40% SOC or 60% SOC straight (Groups D and F in Table 1 and Table S1). After charging (or lithiation), a 30-min rest is allowed for plated Li to chemically intercalate into the graphite and capture the resultant dOCV.dt^{-1}. Following the rest, cells were discharged (delithiated) at C/5. The discharge dQ.dV^{-1} curves are shown Figure S8.

Key results are summarized in Figure 3. A distinct reduction in CE is observed for both SOC (60% and 40%) conditions as shown in Figures 3A and 3D, indicating low reversibility of plated Li as discussed earlier. A dOCV.dt^{-1} plateau related to Li plating is observed within a few cycles for both SOC cases, which, however, shows distinct variability between cells within the same group. For instance, the cell that has lower CE for the 6C- 60% SOC case, i.e., cell 1 in Figure 3A, shows one dOCV.dt^{-1} plateau at around 5 min (Figure 3B), whereas the other cell with slightly higher CE (i.e., Cell 2) shows two distinct peaks—one early narrow peak before 5 min and another broader one at around 15 min (Fig. 3C). In both cases, the initial sharp peak can be attributed to inhomogeneous graphite phases associated with different degree of graphite lithiation and the later broader peak can be due to mixed equilibrium potentials between Li^0/Li^+ and Li_xC_6/Li^+ [6, 7]. The lower extent of lithiation at 6C (6C-40% SOC) showed similar behavior (Figures 3D, E and F). Nevertheless, the presence of dOCV.dt^{-1} plateau clearly indicates chemical lithiation of plated Li during rest (see Figure S8 for additional evidence of chemical intercalation).

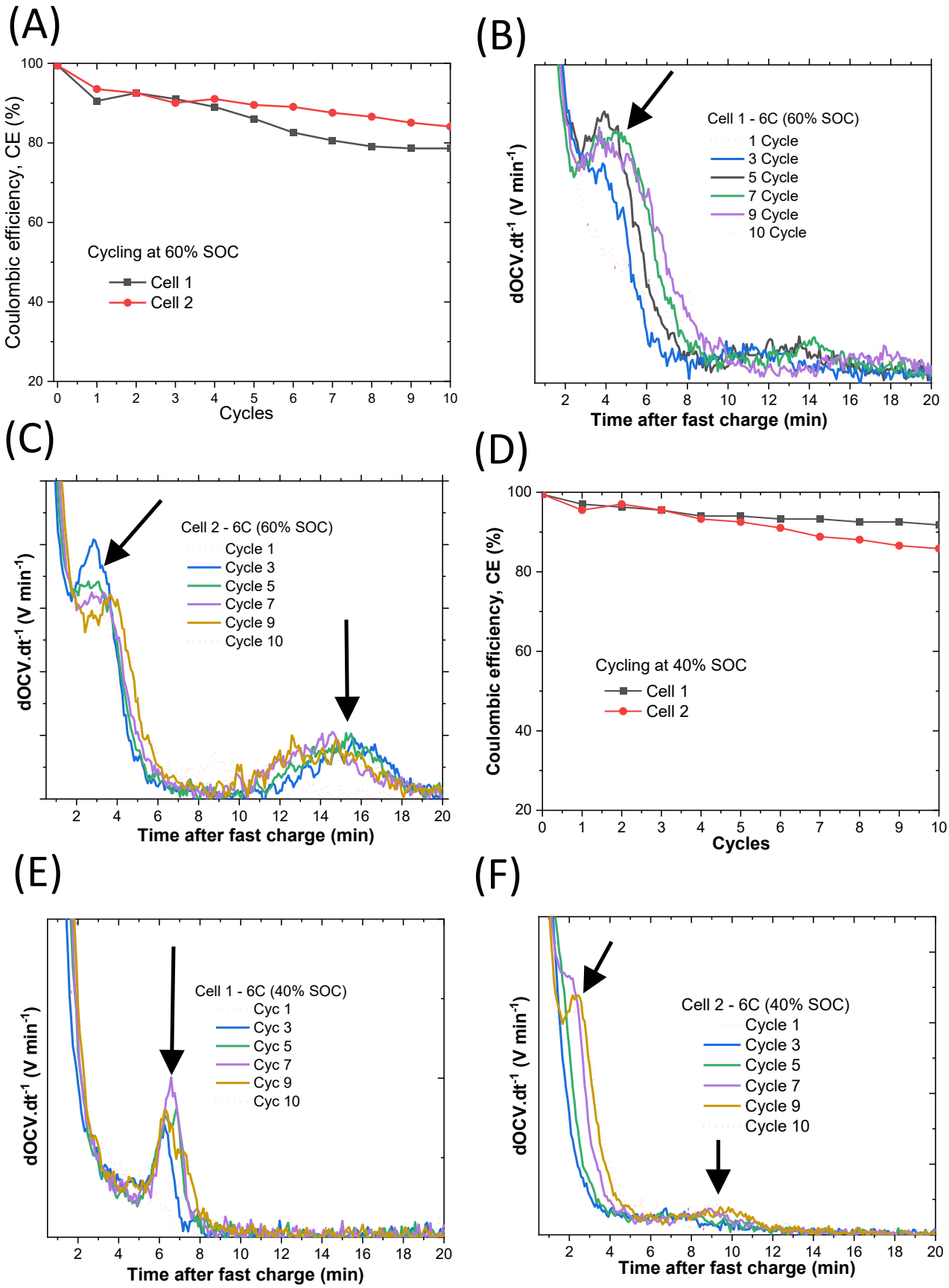
(A)
Coulombic efficiency, CE (%)
Cycles
Cycling at 60% SOC
Cell 1
Cell 2
(B)
dOCV.dt-1 (V min-1)
Time after fast charge (min)
Cell 1 - 6C (60% SOC)
1 Cycle
3 Cycle
5 Cycle
7 Cycle
9 Cycle
10 Cycle
(C)
dOCV.dt-1 (V min-1)
Time after fast charge (min)
Cell 2 - 6C (60% SOC)
Cycle 1
Cycle 3
Cycle 5
Cycle 7
Cycle 9
Cycle 10
(D)
Coulombic efficiency, CE (%)
Cycles
Cycling at 40% SOC
Cell 1
Cell 2
(E)
dOCV.dt-1 (V min-1)
Time after fast charge (min)
Cell 1 - 6C (40% SOC)
Cyc 1
Cyc 3
Cyc 5
Cyc 7
Cyc 9
Cyc 10
(F)
dOCV.dt-1 (V min-1)
Time after fast charge (min)
Cell 2 - 6C (40% SOC)
Cycle 1
Cycle 3
Cycle 5
Cycle 7
Cycle 9
Cycle 10

Figure 3. A) CE for Li/graphite half-cells at 6C charge to 60 SOC% with 30 minutes rest followed by C/5 discharge B) Differential OCVs extracted from cycling data after 6C charging to 60% SOC (Cell 1). C) Differential OCVs extracted from cycling data after 6C charging to 60% SOC (Cell 2). D) CE for gr/Li half-cells cycling at 6C charge to 40 SOC% with 30 minutes rest followed by C/5 discharge. E) Differential OCVs extracted from cycling data after 6C charging to 40% SOC (Cell 1). F) Differential OCVs extracted from cycling data after 6C charging to 40% SOC (Cell 2). The arrow(s) shows mixed phases and dual-plateau signature.

We cycled additional cells to capture the emergence of the $dOCV.dt^{-1}$ signature at XFC condition—in other words, at what minimum SOC we can see the CI related $dOCV.dt^{-1}$ signature first and whether the emergence was consistent. A second reason was to capture the effect of cycling parameter such as alternating rest and no rest after charging on $dOCV.dt^{-1}$ signature. These two tests were combined into one. For evaluating the emergence of the $dOCV.dt^{-1}$ signature, we performed an SOC sweep at 6C from 20% to either 40% or 60% SOC with 5% increments in each cycle (Table1 and Table S1, Groups A and B). Upon performing the SOC sweep up to either 40 or 60% SOC, an additional 10 cycles were carried out at either 40 or 60% SOC with alternating rest and no rest after charging—i.e., one cycle with rest after charge and another without rest after charge (20 cycles total) that followed a C/5 discharge to 0.005 V. The results are summarized in Figures 4 and S9.

The CE of the 6C charge, with incremental SOC up to 40 and 60% conditions, is shown in Figure 4A. CE starts to decrease noticeably at or beyond 25% SOC due to Li plating (Figure 4A), but does not show clear $dOCV.dt^{-1}$ plateau until 40% SOC (Figure S9A). Cells with 20–60% incremental SOC show dual signature as early as 25% SOC (Figure S9B), but the plateau disappears in the subsequent incremental SOC cycles, from 30 to 60%, even though CE and voltage versus lithiated capacity (Figure S4A) confirm significant Li plating. The uncertainty in $dOCV.dt^{-1}$ signatures between 6C (20–40% SOC) and 6C (20–60% SOC) could be due to cell-to-cell $dOCV.dt^{-1}$ variability [31] and 1st cycle uncertainty at same SOC.

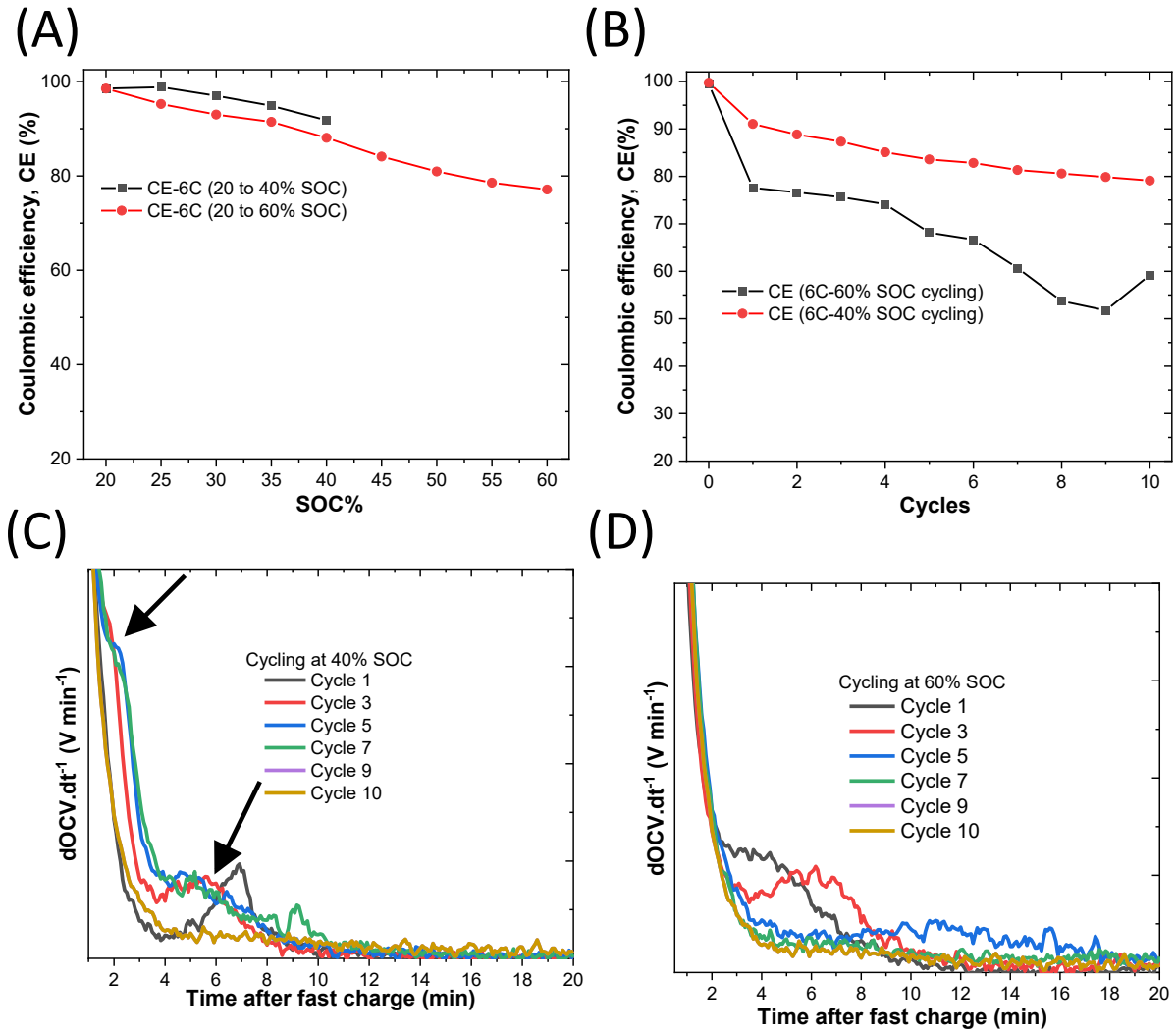

Figure 4. A) CE for Li/graphite half-cells at 6C charge 20–40 SOC%, 20–60 SOC% with 30 minutes rest followed by C/5 discharge B) CE for gr/Li half-cells cycling at 6C charge 40 SOC%, 60 SOC%, with 30 minutes rest followed by C/5 discharge. C) Differential OCVs extracted from cycling data after 6C charging to 40% SOC. D) Differential OCVs extracted from cycling data after 6C charging to 60% SOC. The arrows show mixed phases and dual-plateau signature.

The 6C cycling CE comparison for the 40 and 60% SOCs cases is presented in Figure 4B. In line with previous observations, the CE, lower at 60% SOC than at 40% SOC, confirms that more Li plating occurs at 60% SOC. Cycling at 40% SOC (Figure 4C) shows a sharp $dOCV.dt^{-1}$ signature at Cycle 1 that moves to lower relaxation times with broader peaks followed by an additional small hump between Cycles 2 and 7 (the arrow points to these humps at around 3 min). The $dOCV.dt^{-1}$ signatures at 6C-60% SOC (Figure 4D) are broader than 6C-40% SOC (Figure 4C) and move to

higher relaxation time with cycling. The broader peaks, shifting to higher relaxation times can be attributed to more Li intercalation into graphite to reach the pure Li_xC_6 potential [16]. Unlike the straight cycling condition in Figure 3, both early-relaxation humps (short-lived) and $dOCV.dt^{-1}$ dual signature (the later hump) disappear within a few cycles (Figures 4C and 4D), clearly indicating the diminishing CI effect upon cycling, most likely due to blocking of plated Li from being intercalated into graphite with cycling. The possible reason for such blockage is the accumulation of dead Li at the graphite surface reducing intercalation pathways into graphite particles. However, the reported reasons for the disappearance of $dOCV.dt^{-1}$ plateau at low C-rate (at 30°C, low-Li-plating conditions) were increased plated-Li intercalation rate; reduced Li-plating levels [6, 16, 26] are different from disappearance of $dOCV.dt^{-1}$ at XFC conditions.

Plating at moderate C-rate shows interesting trends in the $dOCV.dt^{-1}$ signature. Figures S10 and S11 present $dOCV.dt^{-1}$ signatures for 3C-60% [Table 1 and Table S1, Group I] and 1C-110% [Table 1 and Table S1, Group K] plating conditions. For 3C-60% SOC, the $dOCV.dt^{-1}$ signatures are found to be broader with cycling, they gradually move to higher relaxation times with cycling. Unlike the 6C cases, the $dOCV.dt^{-1}$ plateau remains visible even after 45 continuous cycles. Konz et al. reported a plating-induced $dOCV.dt^{-1}$ plateau for 3C-50% SOC up to ~30 cycles [7]. Low C-rate and low SOC plate less Li and reduce electrolyte reduction, which further decreases dead Li accumulation (and delays the blockage effect) with cycling. This may be key to see a long term $dOCV.dt^{-1}$ signal. Interestingly, no plating-related $dOCV.dt^{-1}$ plateau is observed during rest for the 1C-110% SOC plating condition (Fig. S11) up to 30 cycles. At the end of rest during discharge, distinct and stable Li-stripping $dQ.dV^{-1}$ signatures are clearly present for 1C-110% SOC case. This indicates that the reversible portion of the plated Li couldn't chemically intercalate into the fully lithiated graphite. The presence of CI-related $dOCV.dt^{-1}$ (Figure S10) peak and absence of stripping-related $dQ.dV^{-1}$ signature (S12B) for the 3C-60% SOC case can primarily be attributed to the partially lithiated graphite that had additional space to accommodate the CI process. Therefore, the EC $dOCV.dt^{-1}$ Li plating signature is sensitive to the amount of plated Li, which depends on charging rate, SOC and cycling history.

Figure S13 compares CE of cells (from groups C, D,E, F, G, H, I and J in Tables 1 and S1) with and without rest after charge (or lithiation) at different C-rates (1C to 6C). The similar CE in Figure S13 shows the same performance even though Li plating under XFC was not detectable with the $dQ.dV^{-1}$ technique. The $dOCV.dt^{-1}$ signature shows evidence of Li plating at XFC conditions with some

variability and disappears with cycling (more Li plating). The dOCV.dt^{-1} Li plating signature was not found at 1C-110% SOC, even with significant Li plating due to the lack of the mixed potential effect between fully lithiated graphite and plated Li.

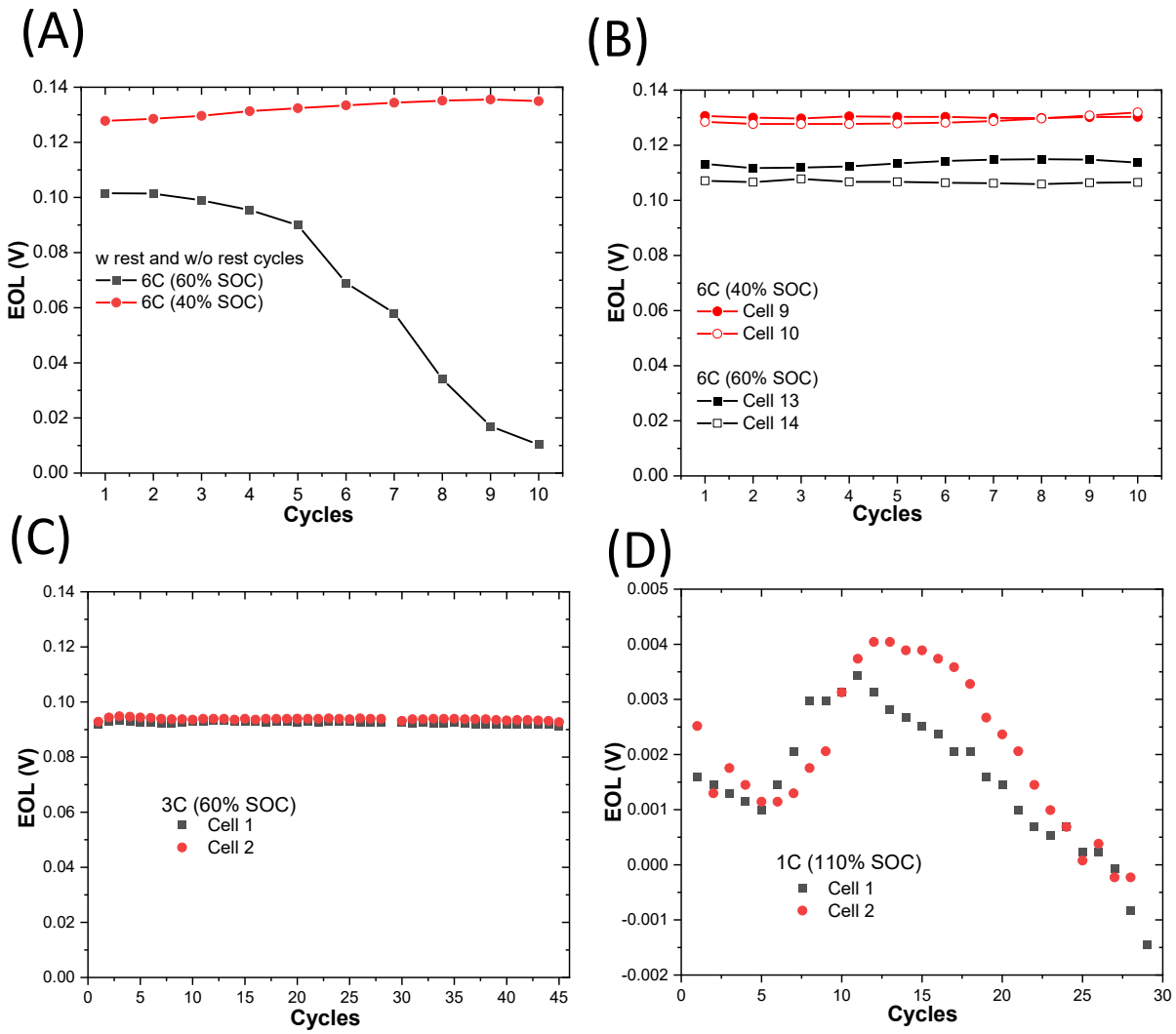

Figure 5. A) End of lithiation (EOL) rest-voltage profiles of Li/graphite half-cells after charging at 6C charge to 60 SOC% after incremental capacity with 30 minutes rest and 6C charge to 40 SOC% after incremental capacity with 30 minutes rest. B) EOL rest-voltage profiles of Li/graphite cells after charging at 6C charge to 60 SOC% with 30 minutes rest and 6C charge to 40 SOC% with 30 minutes rest. C) EOL rest voltage profiles of Cells 3 and 4 after charging at 3C charge to 60 SOC% after 30 minutes rest. D) EOL rest-voltage profiles of Cells 5 and 6 after charging at 1C charge to 110 SOC% after 30 minutes rest.

End of lithiation rest voltage. Earlier research has identified increasing trend of end of charge (EOC) rest voltage in full cells as indicative of Li plating [3, 31]. An increasing trend in full-cell EOC rest voltage captures the mixed potential effect between Li and graphite that, upon plating, could settle to a lower anode EOL rest voltage. Here we evaluate the sensitivity of EOC or EOL rest voltage under XFC Li plating conditions in half cells—i.e., for different charging rates and extent of lithiation (or SOC). Note the voltage measurement resolution is 2 mV.

Figure 5A presents the cycle-by-cycle EOL rest voltage at 6C rate and up to different extents of lithiation—i.e., up to 40 or 60% SOC (Table S1, Group A and B). Note that these cells have gone through incremental SOC tests up to either 40 or 60% SOC at the same rate before cycling (or Cycle 1). Figure 5B shows the EOL rest voltage for the directly cycled cells (without incremental SOC) at 6C up to either 40 or 60% SOC (Group D and F in Tables 1 and S1). Figure 5C shows the EOL rest voltage for moderate charge rate—i.e., 3C up to 60% (Group I in Table 1 and Table S1)—and Figure 5D shows the EOL rest voltage for 1C-110% lithiation case (Group K in Table 1 and Table S1).

A quick examination of Figures 5A-D reveal that early-cycle EOL rest voltages settle to a lower value with decreased C-rate and/or higher SOC, primarily due to reaching higher extent of lithiation (lower polarization at lower rate and/or higher lithiation due to higher SOC). Upon cycling, the 6C cells show distinct behavior depending on their prior history. A decrease in EOL voltage is only visible in the 6C-60% condition that went through incremental SOC cycling before between 20 and 60%, and it is evident from Figures4 (A) and S9B that extensive Li plating had already happened during that period. Therefore, unlike the 6C-60% SOC case without prior incremental SOC cycling in Figure 4B, the 6C-60% case with incremental SOC cycling in Figure 4A has started cycling with plating. The EOL rest voltage for 6C-40% SOC with prior incremental SOC cycling (Figure 5A), and 6C-60% and 6C-40% (Figure 5B) without incremental SOC cycling remain nearly flat with cycling, up to 10 cycles. A similar pattern can also be observed for 3C-60% SOC EOL rest voltage. However, EOL rest voltage for 1C-110% SOC showed a slightly decreasing trend with continued cycling.

Several competing factors that dictate the evolution of EOL rest voltage could be at play. The 6C-60% SOC condition that went through incremental SOC cycling, suffered extensive Li plating and consequent irreversible loss of Li, as shown in Figure S5A to S5C. This is evident in Figure S5D, which shows distinct decrease in graphite Stage II and III $dQ.dV^{-1}$ peak intensity. These almost disappear after five cycles, confirming less utilization or activity of graphite due to the blockage

effect. The disappearance of $dOCV.dt^{-1}$ plateau in Figure 4D after five cycles further confirms the blockage effect that diminished the Li CI process. The diminished CI essentially inhibits graphite voltage to go up through higher utilization. Therefore, under this aggressive plating condition, the graphite gradually loses its characteristics and turns into a Li electrode, consequently making the cell behave like a Li/Li symmetric cell. The symmetric cell behavior is visible at Cycle 10 in Figure S5D, which shows completely suppressed graphite $dQ.dV^{-1}$ peaks and the emergence of a new peak around 0.05 V. The symmetric cell behavior reflects as gradually reduced EOL voltage in Figure 5A. The blockage effect is not yet dominant within 10 cycles for the cells cycled at 6C-40% SOC (with prior incremental SOC cycling), 6C-60% SOC and 6C-40% SOC (straight cycling), and 3C-60% SOC as shown in Figures S10 A, B and S12 B. As a result, the EOL voltage still remains flat for those conditions up to 10 cycles. For the 1C-110% condition, a slight decrease in EOL voltage after Cycle 12 could also be attributed to diminished Li CI, but is due to full graphite utilization.

Therefore, the cycle-by-cycle evolution of EOL rest voltage depends on the condition of graphite upon plating and may not be visible until sufficient blockage by irreversible plated Li has created and diminished the CI pathways of plated Li.

CONCLUSIONS

We have established that the $dQ.dV^{-1}$ Li-plating signature is an unreliable detection signature for fast charging conditions (e.g., 3C to 6C). However, the same signature is a reliable one for low charging conditions (e.g., 1C). This is primarily because of the distinct reversibility behavior of plated Li at different charging rates. To the best of our knowledge, the current literature do not have a methodical study on the effect of C-rate on lithium reversibility to bring out this dependency. And as a result, too often many researchers and diagnostic end users overlook this dependency, and thereby gravitate to misguided or incomplete conclusions. This study will remove this gap in understanding and help to develop better diagnostics. Plating at higher rates (3C and 6C) between 20 and 60% SOC shows no Li-stripping $dQ.dV^{-1}$ signature. At these conditions, large negative overpotentials promote less graphite utilization and more Li plating. However, most of the plated Li becomes irreversible because of either forming dead Li or reacting with electrolyte. A certain fraction of plated Li intercalates back to graphite chemically during plating. The combined effect is meager stripping efficiency (~20%) and non-existent $dQ.dV^{-1}$ signature. However, plating at low C-rate (e.g., 1C)

distinctly improves the reversibility behavior by minimizing Li loss and produces very stable Li stripping $dQ.dV^{-1}$ signature until cell failure.

The EC $dOCV.dt^{-1}$ that captures the CI mechanism presents a completely opposite behavior than $dQ.dV^{-1}$. Unlike $dQ.dV^{-1}$ signature, the $dOCV.dt^{-1}$ signature shows up for fast-charging conditions—i.e., at 3C and 6C. However, these signatures disappear in a few cycles upon continuous cycling with more and more Li plating that forms commensurate dead Li and blocks the CI pathways to the graphite. The inherent cell-to-cell variability also affects the $dOCV.dt^{-1}$ signature at the same cycling condition. Most interestingly, no $dOCV.dt^{-1}$ signature shows up for 1C plating condition because the graphite becomes fully lithiated, leaving no room for chemical intercalation. This reversible part of Li that could not able to intercalation later stripped back during discharge, providing distinct $dQ.dV^{-1}$ signature after 30 min rest. To the best of our knowledge, we are the first study to highlight this phenomenon with its relevant test data. The observations re-emphasize the intricate relationship of Li-plating and its reversibility to a graphite state, and how that impacts EC lithium detection signatures.

The EOL rest voltage after charging captures the mixed potential effect between plated Li and graphite. This study shows that EOL voltage only decreased when CI pathways into graphite become blocked (or when no $dOCV.dt^{-1}$ signature is present). Such blockage, as discussed earlier, could happen at XFC conditions. Therefore, the EOL rest-voltage trend should be tracked and verified with $dOCV.dt^{-1}$ signature.

Given the sensitivity and unreliability issues associated with individual signatures under XFC conditions, we suggest tracking multiple detection signatures together like CE, EOC rest voltage, $dOCV.dt^{-1}$, and others concurrently.

ASSOCIATED CONTENT

Supporting Information. Contain detailed EC test matrix, digital photographs, and additional EC cycling results.

AUTHOR INFORMATION

Corresponding Author

Tanvir R. Tanim, Tanvir.Tanim@inl.gov

Author Contributions

PRC, TRT and EJD contributed to conceptualization, PRC prepared cells and PRC, CD performed data acquisition. PRC performed electrochemical analysis. ML assisted data capture and analysis. PRC and TRT performed original manuscript preparation. All authors contributed to the review and discussion of results.

ACKNOWLEDGMENT/ FUNDING SOURCES

Funding provided by the Vehicle Technologies Office of the U.S. Department of Energy's Office of Energy Efficiency and Renewable Energy under the guidance of the Advanced Battery Cell Research Program (eXtreme fast charge Cell Evaluation of Lithium-ion batteries – XCEL). This manuscript has been authored by Battelle Energy Alliance, LLC under Contract No. DE-AC07-05ID14517 for Idaho National Laboratory with the U.S. Department of Energy. The United States Government retains and the publisher, by accepting the article for publication, acknowledges that the United States Government retains a non-exclusive, paid-up, irrevocable, worldwide license to publish or reproduce the published form of this manuscript, or allow others to do so, for United States Government purposes. The authors thank Samuel Gillard from the U.S. Department of Energy for supporting this project. The authors thank CAMP facility for providing graphite electrodes.

Notes. The authors declare no competing interests.

ABBREVIATIONS

XFC: Extreme fast charging, EC: Electrochemical, CC: Constant current, EOL: End of lithiation, dOCV: Differential open circuit voltage, SOC: State of charge, SEI: Solid electrolyte interphase, Li: Lithium.

REFERENCES

1. Christopher Michelbacher, S.A., Ira Bloom, Andrew Burnham, Barney Carlson, Fernando Dias, Eric J Dufek, Andrew N Jansen, Matthew Keyser, Anthony Markel, Andrew Meintz, Manish Mohanpurkar, Ahmad Pesaran, Don Scoffield, Matthew Shirk, Thomas Stephens, Tanvir Tanim, Ram Vijayagopal, Jiucai Zhang, *Enabling fast charging–Introduction and overview.* Journal of Power Sources. **367**(NREL/JA-5400-69053; INL/JOU-18-45158-Rev000).
2. Ahmed, S., et al., *Enabling fast charging – A battery technology gap assessment.* Journal of Power Sources, 2017. **367**: p. 250-262.
3. Tanim, T.R., et al., *Heterogeneous Behavior of Lithium Plating during Extreme Fast Charging.* Cell Reports Physical Science, 2020. **1**(7): p. 100114.
4. Anseán, D., et al., *Operando lithium plating quantification and early detection of a commercial LiFePO4 cell cycled under dynamic driving schedule.* Journal of Power Sources, 2017. **356**: p. 36-46.
5. Burns, J.C., D.A. Stevens, and J.R. Dahn, *In-Situ Detection of Lithium Plating Using High Precision Coulometry.* Journal of The Electrochemical Society, 2015. **162**(6): p. A959-A964.
6. Uhlmann, C., et al., *In situ detection of lithium metal plating on graphite in experimental cells.* Journal of Power Sources, 2015. **279**: p. 428-438.
7. Konz, Z.M., E.J. McShane, and B.D. McCloskey, *Detecting the Onset of Lithium Plating and Monitoring Fast Charging Performance with Voltage Relaxation.* ACS Energy Letters, 2020. **5**(6): p. 1750-1757.
8. Paul, P.P., et al., *A Review of Existing and Emerging Methods for Lithium Detection and Characterization in Li-Ion and Li-Metal Batteries.* Advanced Energy Materials, 2021. **11**(17): p. 2100372.
9. Tanim, T.R., et al., *Electrochemical Quantification of Lithium Plating: Challenges and Considerations.* Journal of The Electrochemical Society, 2019. **166**(12): p. A2689-A2696.
10. Zinth, V., et al., *Lithium plating in lithium-ion batteries at sub-ambient temperatures investigated by in situ neutron diffraction.* Journal of Power Sources, 2014. **271**: p. 152-159.
11. Petzl, M. and M.A. Danzer, *Nondestructive detection, characterization, and quantification of lithium plating in commercial lithium-ion batteries.* Journal of Power Sources, 2014. **254**: p. 80-87.
12. von Lüders, C., et al., *Lithium plating in lithium-ion batteries investigated by voltage relaxation and in situ neutron diffraction.* Journal of Power Sources, 2017. **342**: p. 17-23.

13. Campbell, I.D., et al., *How Observable Is Lithium Plating? Differential Voltage Analysis to Identify and Quantify Lithium Plating Following Fast Charging of Cold Lithium-Ion Batteries.* Journal of The Electrochemical Society, 2019. **166**(4): p. A725-A739.
14. Koleti, U.R., et al., *The development of optimal charging strategies for lithium-ion batteries to prevent the onset of lithium plating at low ambient temperatures.* Journal of Energy Storage, 2019. **24**: p. 100798.
15. Koleti, U.R., T.Q. Dinh, and J. Marco, *A new on-line method for lithium plating detection in lithium-ion batteries.* Journal of Power Sources, 2020. **451**: p. 227798.
16. Schindler, S., et al., *Voltage relaxation and impedance spectroscopy as in-operando methods for the detection of lithium plating on graphitic anodes in commercial lithium-ion cells.* Journal of Power Sources, 2016. **304**: p. 170-180.
17. Carter, R., et al., *Detection of Lithium Plating During Thermally Transient Charging of Li-Ion Batteries.* Frontiers in Energy Research, 2019. **7**(144).
18. Kim, C.-S., et al., *Effects of Capacity Ratios between Anode and Cathode on Electrochemical Properties for Lithium Polymer Batteries.* Electrochimica Acta, 2015. **155**: p. 431-436.
19. Bugga, R.V. and M.C. Smart, *Lithium Plating Behavior in Lithium-Ion Cells.* ECS Transactions, 2019. **25**(36): p. 241-252.
20. Keyser, M., et al., *Enabling fast charging – Battery thermal considerations.* Journal of Power Sources, 2017. **367**: p. 228-236.
21. Santhanagopalan, S., P. Ramadass, and J. Zhang, *Analysis of internal short-circuit in a lithium ion cell.* Journal of Power Sources, 2009. **194**(1): p. 550-557.
22. Xiao, J., et al., *Understanding and applying coulombic efficiency in lithium metal batteries.* Nature Energy, 2020. **5**(8): p. 561-568.
23. Downie, L.E., et al., *In Situ Detection of Lithium Plating on Graphite Electrodes by Electrochemical Calorimetry.* Journal of The Electrochemical Society, 2013. **160**(4): p. A588-A594.
24. Waldmann, T., et al., *Interplay of Operational Parameters on Lithium Deposition in Lithium-Ion Cells: Systematic Measurements with Reconstructed 3-Electrode Pouch Full Cells.* Journal of The Electrochemical Society, 2016. **163**(7): p. A1232-A1238.
25. Colclasure, A.M., et al., *Electrode scale and electrolyte transport effects on extreme fast charging of lithium-ion cells.* Electrochimica Acta, 2020. **337**: p. 135854.

26. Chinnam, P., et al., *Fast charging aging considerations: Incorporation and alignment of cell design and material degradation pathways*. 2021. **4** (9): p. 9133-9143
27. Arora, P., M. Doyle, and R.E. White, *Mathematical Modeling of the Lithium Deposition Overcharge Reaction in Lithium-Ion Batteries Using Carbon-Based Negative Electrodes.* Journal of The Electrochemical Society, 1999. **146**(10): p. 3543-3553.
28. Yoon, G., et al., *Deposition and Stripping Behavior of Lithium Metal in Electrochemical System: Continuum Mechanics Study.* Chemistry of Materials, 2018. **30**(19): p. 6769-6776.
29. Vetter, J., et al., *Ageing mechanisms in lithium-ion batteries.* Journal of Power Sources, 2005. **147**(1): p. 269-281.
30. Paul, P.P., *Quantification of heterogeneous, irreversible lithium plating in extreme fast charging of Li-ion batteries.* Energy Environ. Sci. Energy Environ. Sci., 2021. **14**: p. 4979-4988.
31. Chen, B.-R., et al., *A machine learning framework for early detection of lithium plating combining multiple physics-based electrochemical signatures.* Cell Reports Physical Science, 2021: p. 100352.

Supplementary information for

Sensitivity and Reliability of Key Electrochemical Markers for Detecting Lithium Plating during Extreme Fast Charging

Parameswara R. Chinnam[1], Tanvir R. Tanim[2,*], Eric J. Dufek[2] , Charles C. Dickerson[2] and Meng Li[2]

[1] Previous INL employee and currently at Rivian

[2] Energy Storage & Advanced Transportation Department, Idaho National Laboratory, Idaho Falls, ID 83415

[*]Corresponding author

Table T1: Experimental test matrix. All discharge (or delithiation) were performed at C/5 after reaching to the desired SOC.

Group	Test condition	Test details	EC signature
A (3)	6C charge (lithiation) to 20% SOC, followed by up to 60% SOC with 5% increment. Cycling at the same rate at 60% SOC (alternate with rest and no rest after charge)	1. Charge cells to 1.5V at C/10. 2. Rest for 15 min. 3. CC discharge at 6C rate up to y capacity. No lower cutoff voltage limit used. 4. Rest for 30 min (alternate cycles do not have rest), 5. Charge cells to 1.5V at C/5 CC. 6. Rest for 30 min. ** Repeat steps 3-6 for y=20% to 60% SOC at 6C rate with increment of 5% scaled capacity. Note: At each SOC%, perform 2 cycles- 1st one with rest and 2nd one without rest. After reaching 60% SOC, perform 10 cycles with alternative rest and no rest.	Effect of SOC on $dQ.dV^{-1}$, and $dOCV.dt^{-1}$ signatures
B (3)	6C charge to 40% SOC, followed by up to 40% SOC with 5% increment. Cycling at the same rate at 40% SOC (alternate with rest and no rest after charge)	1. Charg cells to 1.5V at C/10. 2. Rest for 15 min. 3. CC discharge at 6C rate up to y capacity. No lower cutoff voltage limit used. 4. Rest for 30 min (alternate cycles do not have rest), 5. Charge cells to 1.5V at C/5 CC. 6. Rest for 30 min. ** Repeat steps 3-6 for y= 20% to 40% SOC at 6C rate with increment of 5% scaled capacity. Note: At each SOC% perform 2 cycles- 1st one with rest and 2nd one without rest. After reaching 40% SOC, perform 10 cycles with alternative rest and no rest.	Effect of SOC on $dQ.dV^{-1}$, and $dOCV.dt^{-1}$ signatures
C (2)	6C charge to 60% SOC. No rest after charge.	1. Charg cells to 1.5V at C/10. 2. Rest for 15 min. 3. CC discharge at 6C rate up to 60% capacity. No lower cutoff voltage limit used. 4. Rest for 0 min 5. Charge cells to 1.5V at C/5 CC. 6. Rest for 30 min. ** Repeat steps 3-6 for 10 times	$dQ.dV^{-1}$ sensitivity and reliability at 6C (60% SOC)
D (2)	6C charge to 60% SOC. 30 min rest after charge.	1. Charg cells to 1.5V at C/10. 2. Rest for 15 min. 3. CC discharge at 6C rate up to 60% capacity. No lower cutoff voltage limit used. 4. Rest for 30 min 5. Charge cells to 1.5V at C/5 CC. 6. Rest for 30 min. ** Repeat steps 3-6 for 10 times	$dOCV.dt^{-1}$ sensitivity and reliability at 6C (60% SOC)
E (2)	6C charge to 40% SOC. No rest after charge.	1. Charg cells to 1.5V at C/10. 2. Rest for 15 min. 3. CC discharge at 6C rate up to 40% capacity. No lower cutoff voltage limit used. 4. Rest for 0 min 5. Charge cells to 1.5V at C/5 CC. 6. Rest for 30 min. ** Repeat steps 3-6 for 10 times	$dQ.dV^{-1}$ sensitivity and reliability at 6C (40% SOC)
F (2)	6C charge to 40% SOC. 30 min rest after charge	1. Charge cells to 1.5V at C/10. 2. Rest for 15 min.	$dOCV.dt^{-1}$ sensitivity and

		3. CC discharge at 6C rate up to 40% capacity. No lower cutoff voltage limit used. 4. Rest for 30 min 5. Charge cells to 1.5V at C/5 CC. 6. Rest for 30 min. ** Repeat steps 3-6 for 10 times	reliability at 6C (40% SOC)
G (2)	1C charge to 110% SOC. No rest after charge.	1. Charge cells to 1.5V at C/10. 2. Rested for 15 min. 3. CC discharge at 6C rate up to 110% capacity. No lower cutoff voltage limit used. 4. Rest for 0 min 5. Charge cells to 1.5V at C/5 CC. 6. Rest for 30 min. ** Repeat steps 3-6 for 10 times	$dQ.dV^{-1}$ sensitivity and reliability at 1C (110% SOC)
H (3)	1C charge to 110% SOC. No rest after charge. Long-term testing	1. Charge cells to 1.5V at C/10. 2. Rest for 15 min. 3. CC discharge at 6C rate up to 110% capacity. No lower cutoff voltage limit used. 4. Rest for 0 min 5. Charge cells to 1.5V at C/5 CC. 6. Rest for 30 min. ** Repeat steps 3-6 for 100 times	Long-term $dQ.dV^{-1}$ sensitivity and reliability at 1C (110% SOC)
I (2)	3C charge to 60% SOC. 30 minutes rest after charge.	1. Charge cells to 1.5V at C/10. 2. Rest for 15 min. 3. CC discharge at 6C rate up to 60% capacity. No lower cutoff voltage limit used. 4. Rest for 30 min 5. Charge cells to 1.5V at C/5 CC. 6. Rest for 30 min. ** Repeat steps 3-6 for 100 times	$dOCV.dt^{-1}$ sensitivity and reliability at 3C (60% SOC)
J (2)	3C charge to 60% SOC. no rest after charge.	1. Charge cells to 1.5V at C/10. 2. Rest for 15 min. 3. CC discharge at 6C rate up to 60% capacity. No lower cutoff voltage limit used. 4. Rest for 0 min 5. Charge cells to 1.5V at C/5 CC. 6. Rest for 30 min. ** Repeat steps 3-6 for 10 times	$dQ.dV^{-1}$ sensitivity and reliability at 3C (60% SOC)
K (2)	1C charge to 110% SOC. 30 min rest after charge *Long-term testing	1. Charge cells to 1.5V at C/10. 2. Rest for 15 min. 3. CC discharge at 6C rate up to 110% capacity. No lower cutoff voltage limit used. 4. Rest for 30 min 5. Charge cells to 1.5V at C/5 CC. 6. Rest for 30 min. ** Repeat steps 3-6 for 100 times	Long-term $dOCV.dt^{-1}$ sensitivity and reliability at 1C (110% SOC)

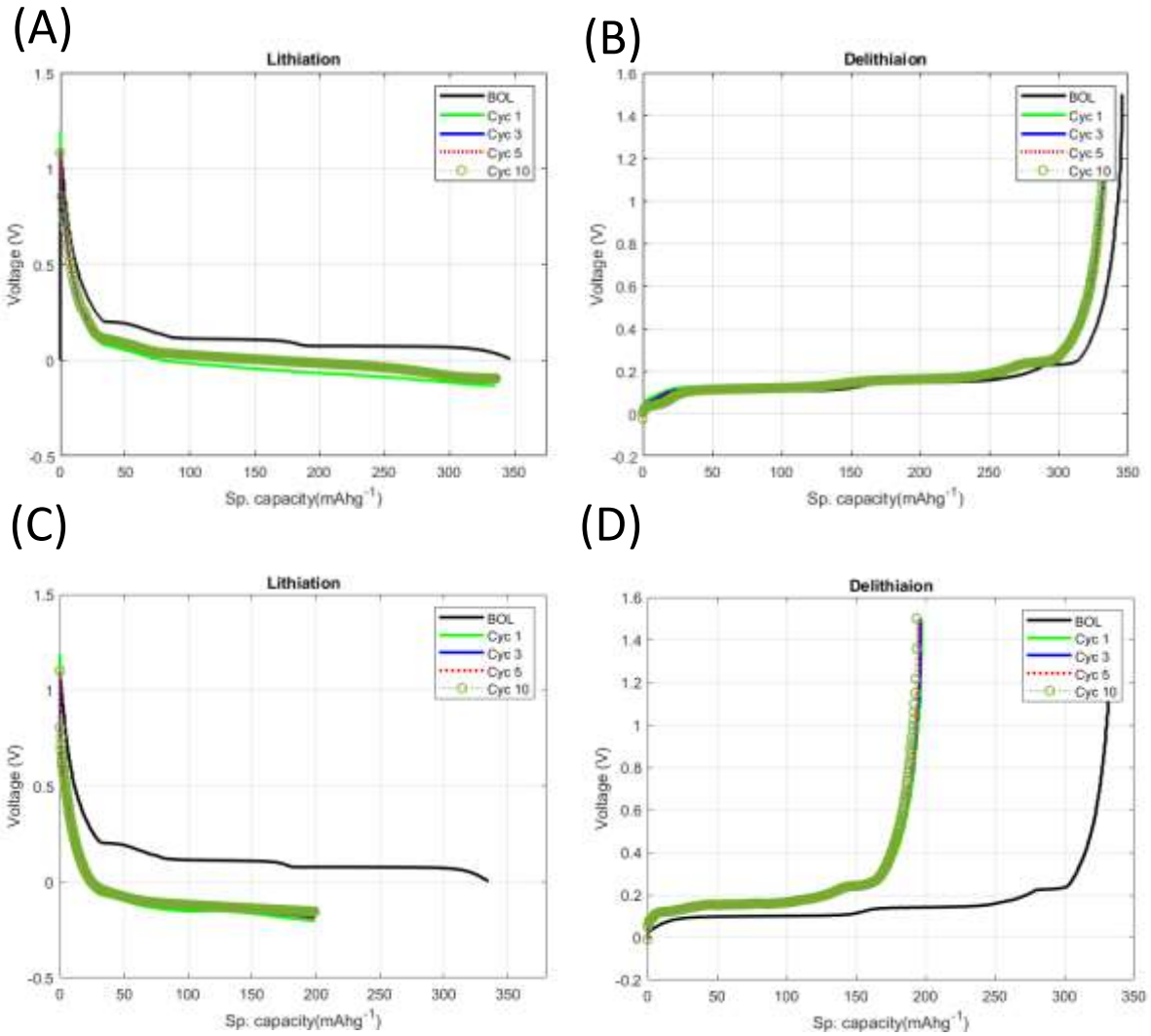

Figure S1. (A) Voltage versus lithiated capacity at 1C and up to 110% SOC (B) voltage versus delithiated capacity at C/5, (C) voltage versus lithiated capacity at 3C and up to 60% SOC, and (D) voltage versus delithiated capacity at 3C and up to 60 % SOC at C/5. Specific capacity is calculated based on mass of graphite.

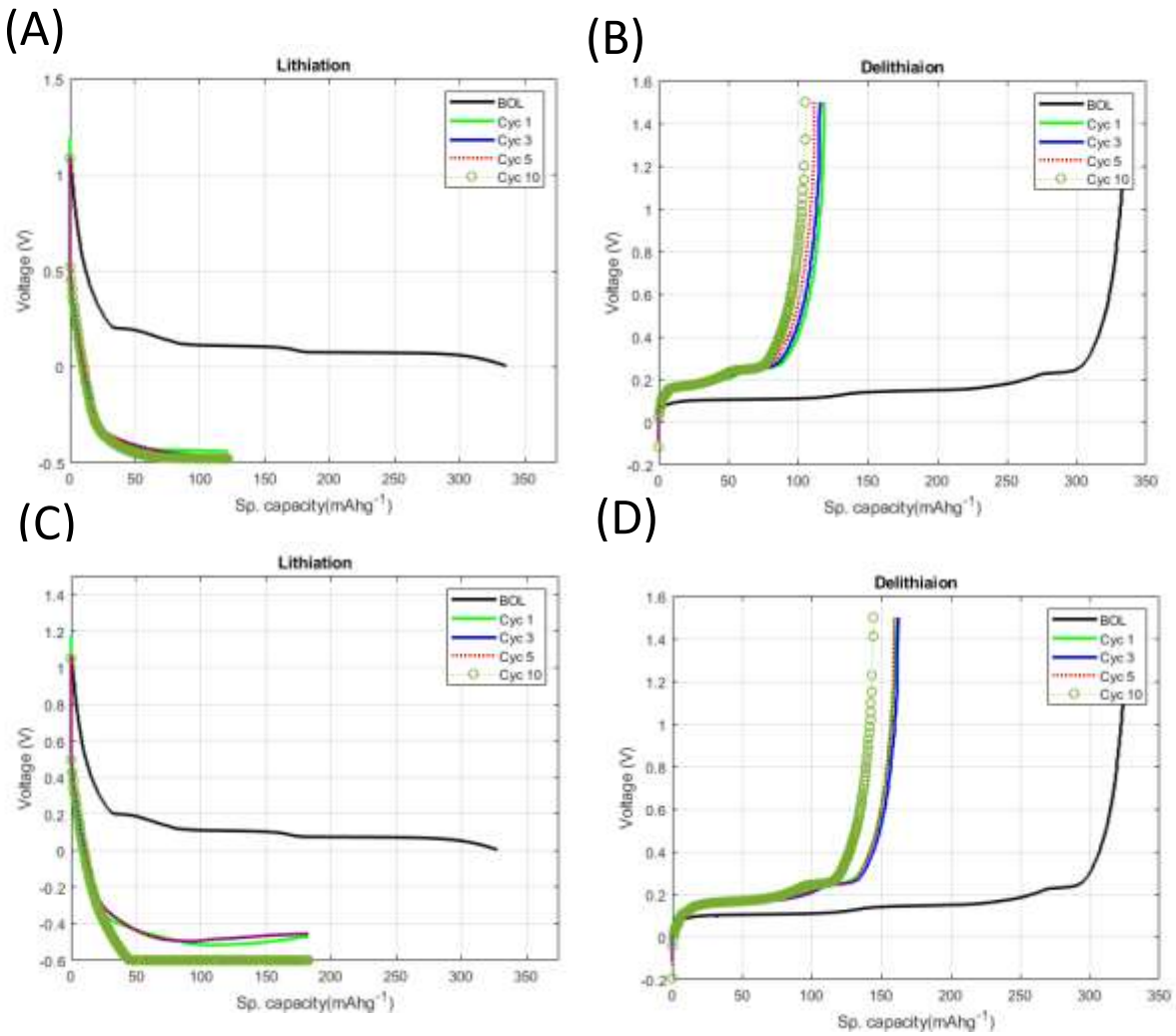

Figure S2. (A) Voltage versus lithiated capacity at 6C and up to 40% SOC, (B) voltage versus delithiated capacity at C/5, (C) voltage versus lithiated capacity at 6C and up to 60% SOC, and (D) voltage versus delithiated capacity at 6C and up to 60 % SOC at C/5. Specific capacity is calculated based on mass of graphite.

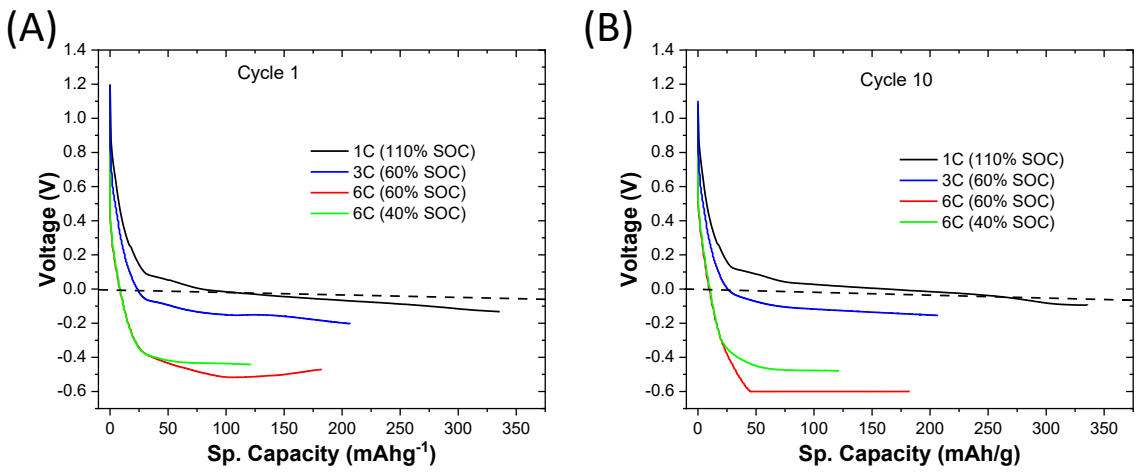

Figure S3. Comparison of cycle 1 voltage versus lithiated capacity at (A) 1C and up to 110% SOC, 3C and up to 60% SOC, 6C and up to 60% SOC and 6C and up to 40% SOC. (B) Comparison of cycle 10 voltage versus lithiated capacity at 1C and up to 110% SOC, 3C and up to 60% SOC, 6C and up to 60% SOC, and 6C and up to 40% SOC. Specific capacity is calculated based on mass of graphite.

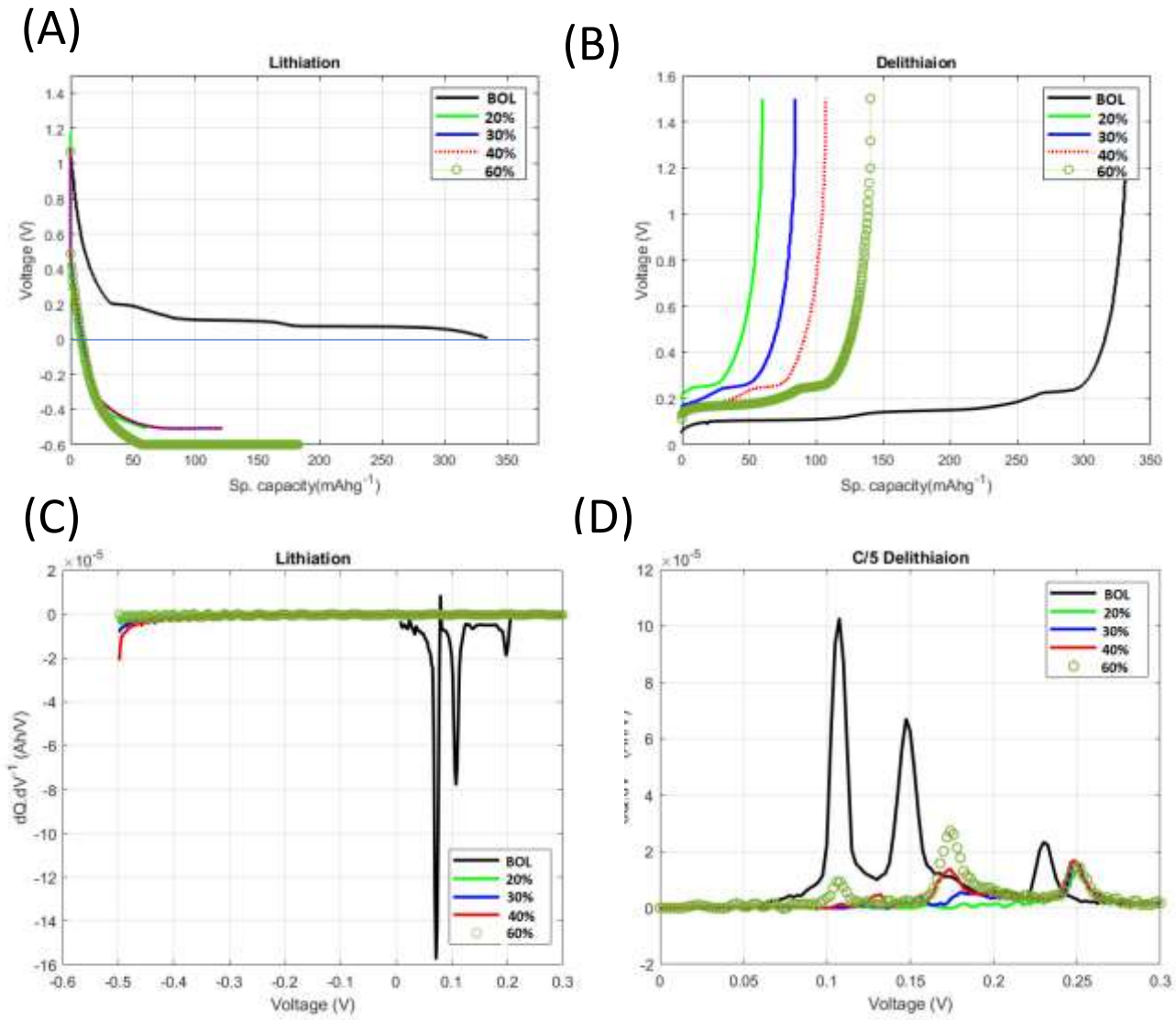

Figure S4. Comparison of voltage versus lithiated capacity at (A) BOL, 6C and up to 20% SOC, 6C and up to 30% SOC, 6C and up to 40% SOC, and 6C and up to 60% SOC. (B) Comparison of voltage versus delithiated capacity at BOL, 6C and up to 20% SOC, 6C and up to 30% SOC, 6C and up to 40% SOC, and 6C and up to 60% SOC. (C) 6C charge $dQ.dV^{-1}$ curves to 20–60% SOC. (D) C/5 discharge $dQ.dV^{-1}$ curves after 6C charging to 20–60% SOC with no rest. Specific capacity is calculated based on mass of graphite.

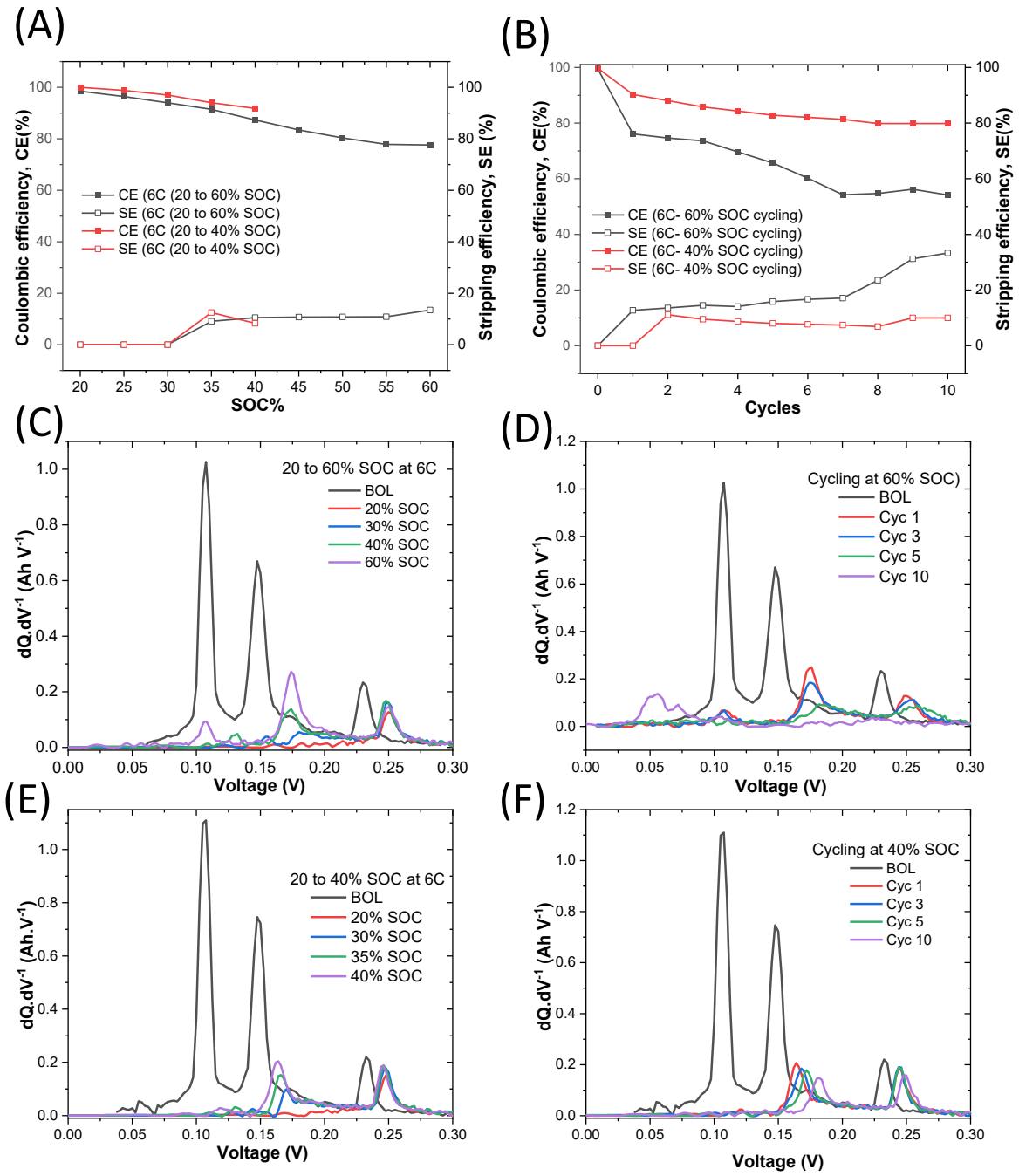

Figure S5. (A) Coulombic and stripping efficiency at 6C charge 20–40 SOC%, 20–60 SOC% with no rest, followed by C/5 discharge. (B) Coulombic and lithium stripping efficiency at 6C charge 40 SOC%, 60 SOC% with no rest followed by C/5 discharge. (C) C/5 discharge $dQ.dV^{-1}$ curves after 6C charging to 20–60% SOC with no rest. (D) C/5 discharge $dQ.dV^{-1}$ curves after 6C charging to 60% SOC with no rest. (E) C/5 discharge $dQ.dV^{-1}$ curves after 6C charging to 20-40% SOC with no rest.

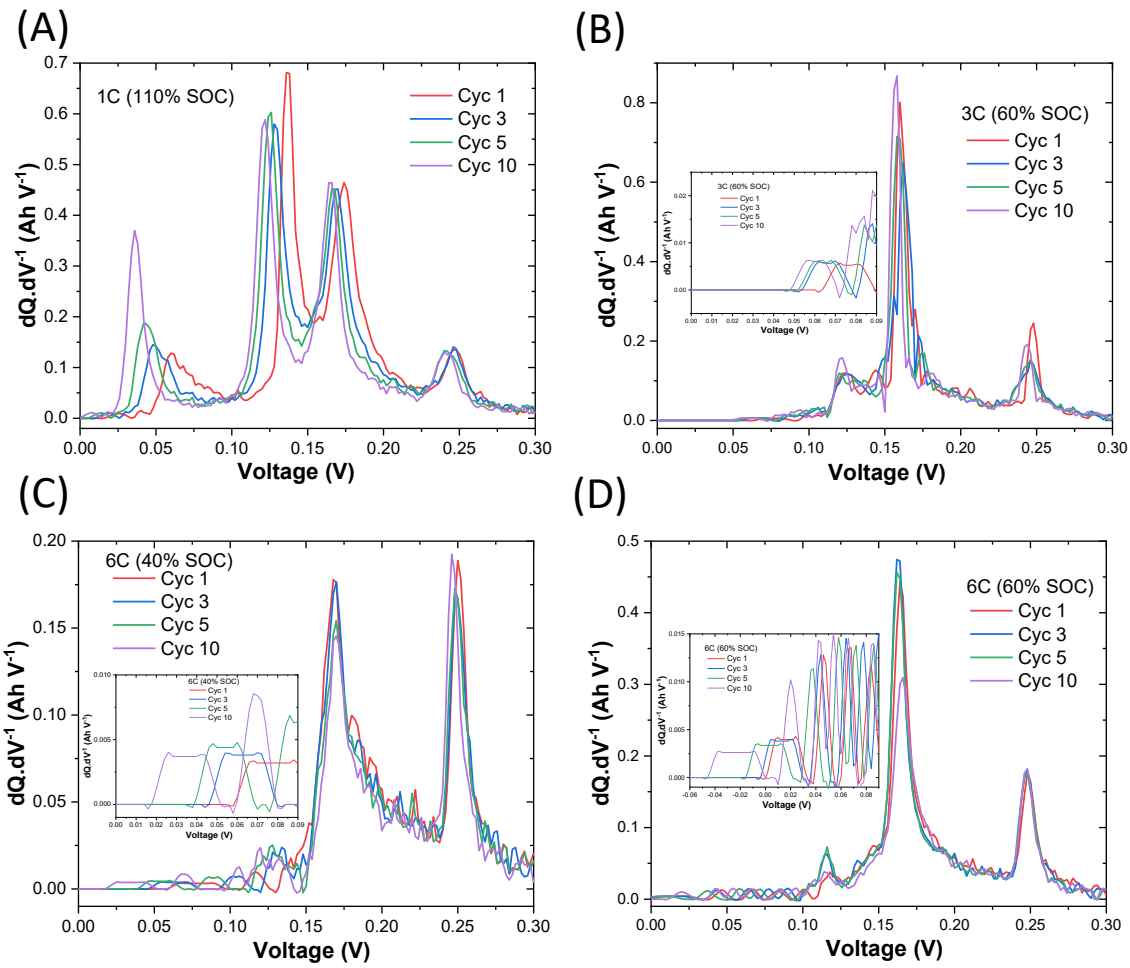

Figure S6. (A) C/5 discharge dQ.dV^{-1} curves after 1C charge 110% SOC with no rest. (B) Discharge dQ.dV^{-1} curves after 3C charge 60% SOC with no rest. (C) Discharge dQ.dV^{-1} curves after 6C charge 40% SOC with no rest. (D) Discharge dQ.dV^{-1} curves after 6C charge 60% SOC with no rest. Note that one cell data from each group is shown at each cycling condition.

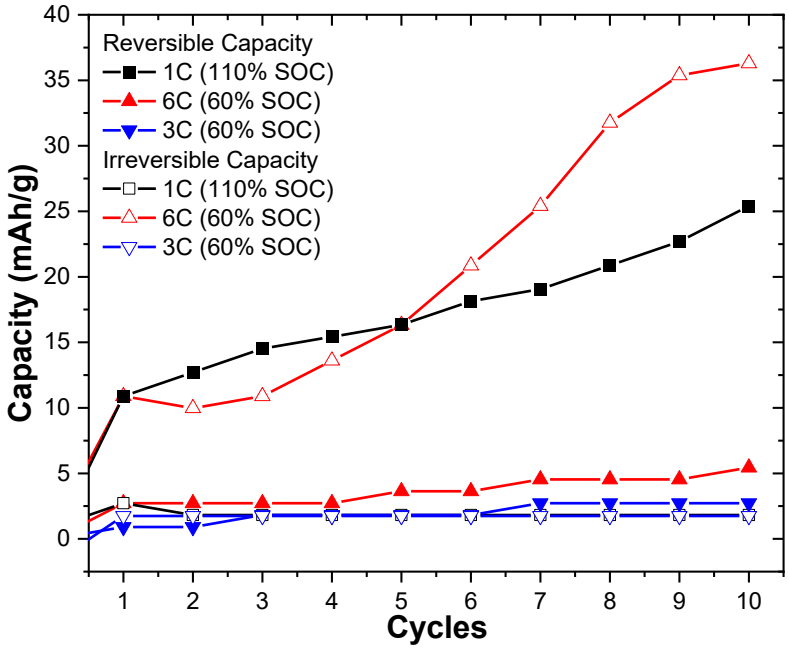

Figure S7. Reversible Li capacity versus irreversible capacity for 1C (110% SOC), 6C (60% SOC) and 3C (60% SOC), as a function of cycles.

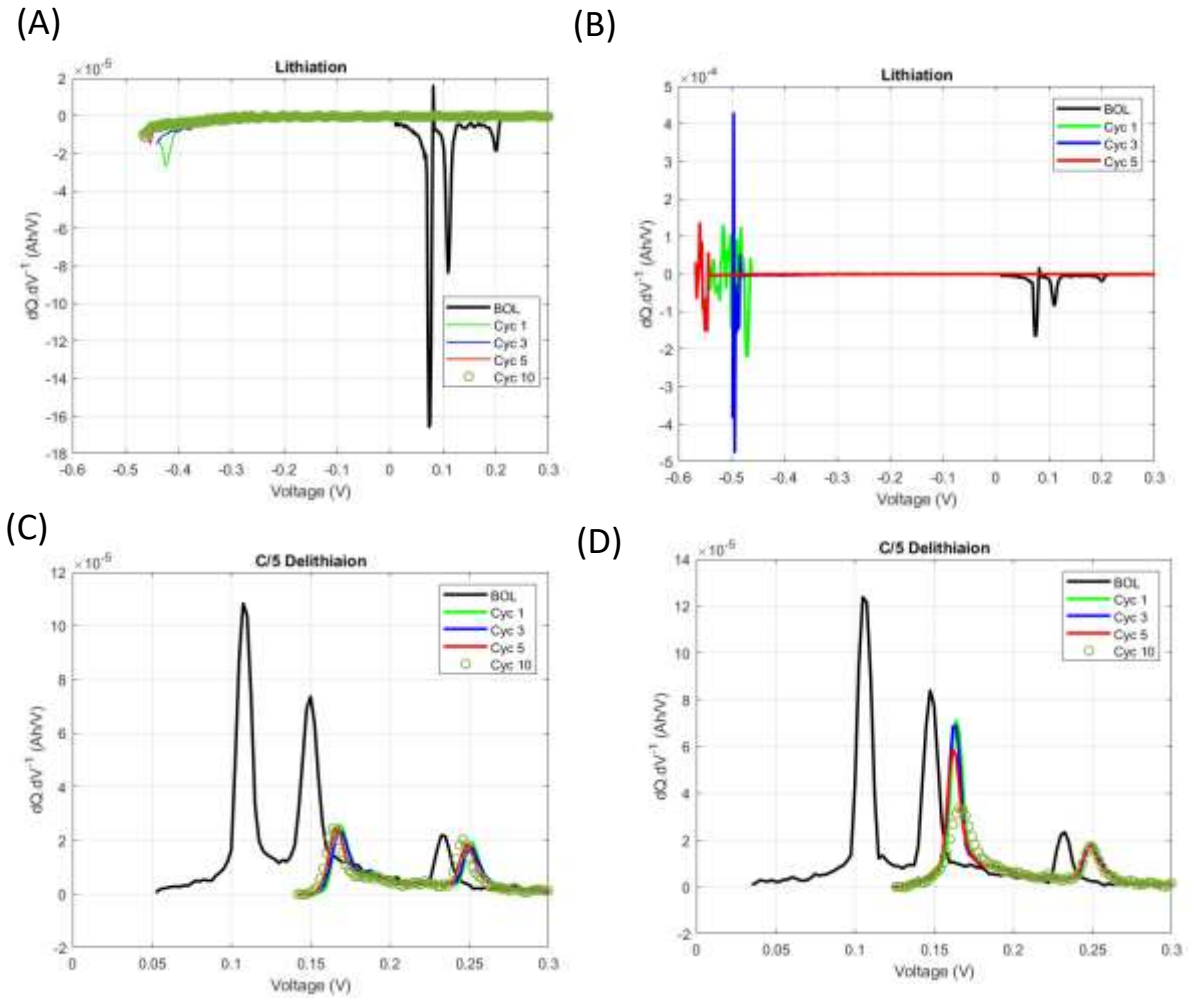

Figure S8 (A) 6C charge dQ.dV^{-1} curves to 40% SOC. (B) 6C charge dQ.dV^{-1} curves to 60% SOC. (C) C/5 discharge dQ.dV^{-1} curves after 6C charge 40% SOC with 30 minutes rest. (D) Discharge dQ.dV^{-1} curves after 6C charge 60% SOC with 30 minutes rest.

The charge dQ.dV^{-1} curves in Figure in S8 A,B show mainly Li plating and no graphite peaks associated with lithiation. The discharge dQ.dV^{-1} curves in Figure S8 C,D shows that discharge starts past the graphite Stage I peak, and the appearance of Stage II and III confirm significant Li chemical intercalation has happened before discharge. The high C-rate conditions favor more Li plating and parallel chemical intercalation into graphite during charge and after charge (rest). This results in dOCV.dt^{-1} plateau during rest, which is highly variable at same cycling conditions.

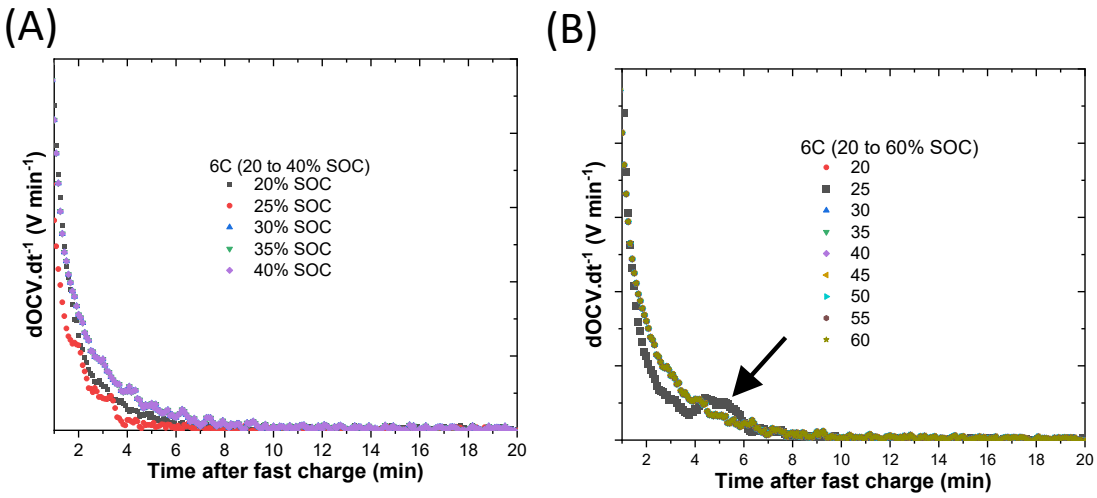

Figure S9. (A) Differential OCVs extracted from cycling data after 6C charging to 20–40% SOC, $dOCV.dt^{-1}$ change not observed from 20–40% SOC. (B) Differential OCVs extracted from cycling data after 6C charging to 20-60% SOC, $dOCV.dt^{-1}$ change observed at 60% SOC. The arrow shows dual-plateau signature.

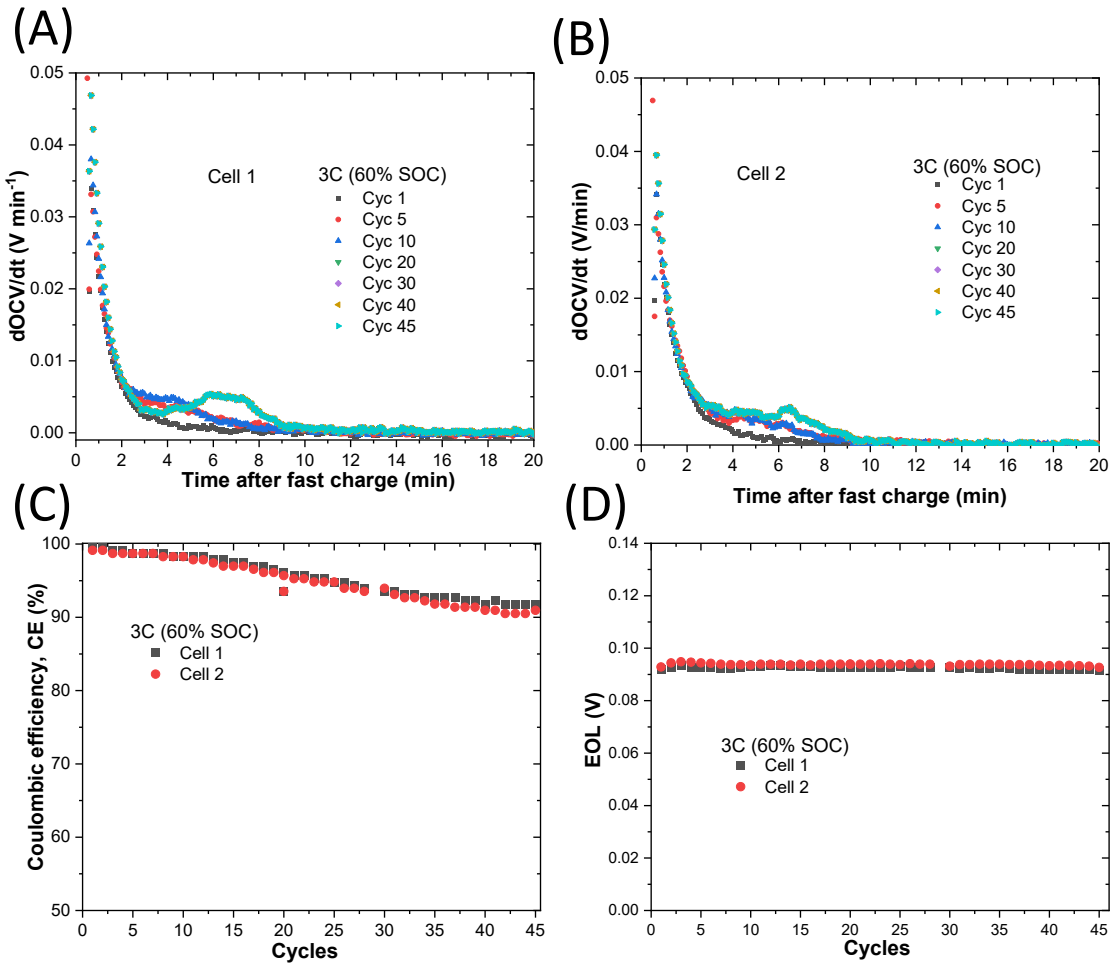

Figure S10. (A) Differential OCVs extracted from cycling data after 3C charging to 60% SOC (Cell 3). (B) Differential OCVs extracted from cycling data after 3C charging to 60% SOC (Cell 4). (C) Coulombic efficiency of Cells 3 and 4 at 3C charge to 60 SOC% with 30 minutes rest followed by C/5 discharge. (D) EOL rest voltage profiles of Cells 3 and 4 after charging at 3C charge to 60 SOC% after 30 minutes rest.

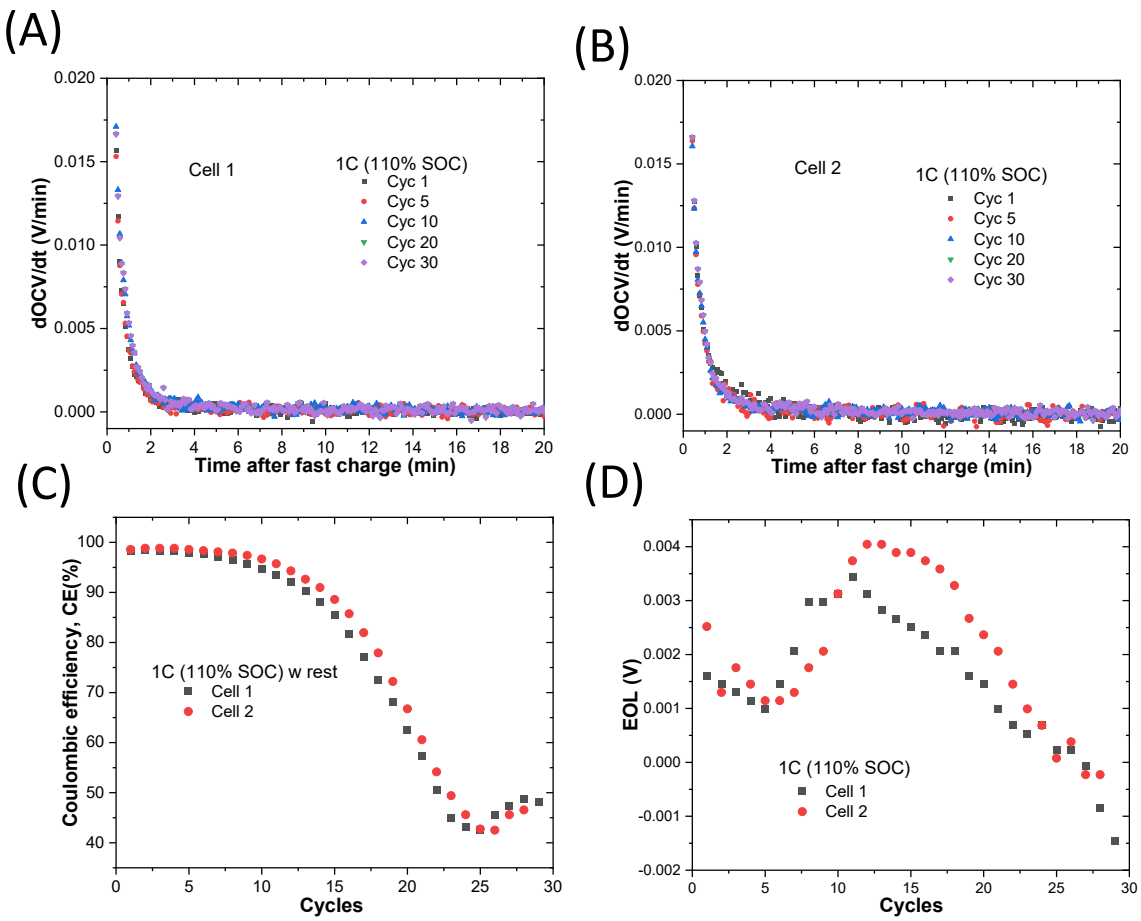

Figure S11. (A) Differential OCVs extracted from cycling data after 1C charging to 110% SOC (Cell 5). (B) Differential OCVs extracted from cycling data after 1C charging to 110% SOC (Cell 6). (C) Coulombic efficiency of Cells 5 and 6 at 1C charge to 110 SOC% with 30 minutes rest followed by C/5 discharge. (D) EOL rest voltage profiles of Cells 5 and 6 after charging at 1C charge to 110 SOC% after 30 minutes rest.

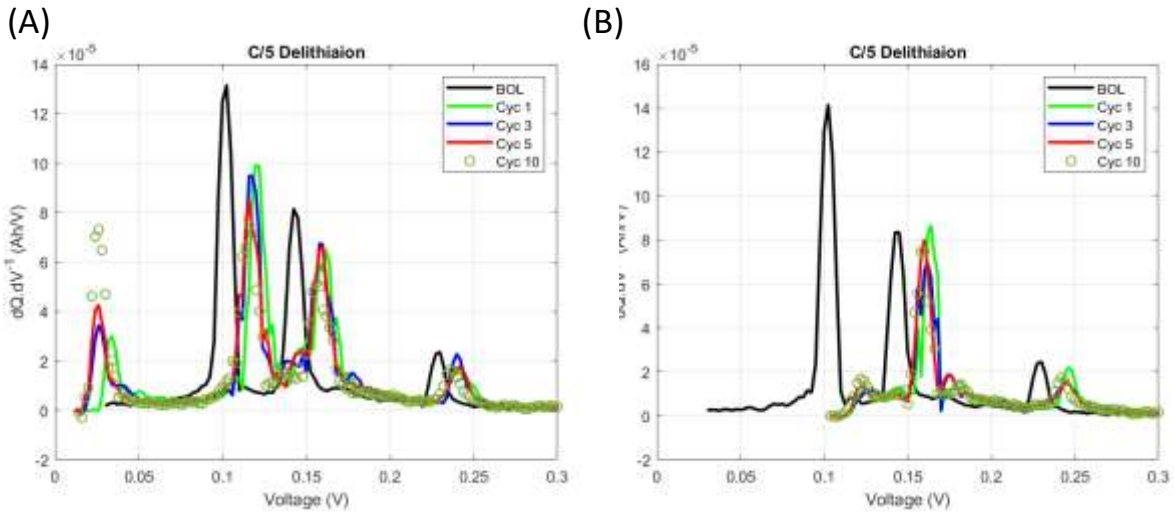

Figure S12. (A) C/5 discharge dQ.dV^{-1} curves after 1C charge 110% SOC with 30 minutes rest. (B) Discharge dQ.dV^{-1} curves after 3C charge 60% SOC with 30 minutes rest.

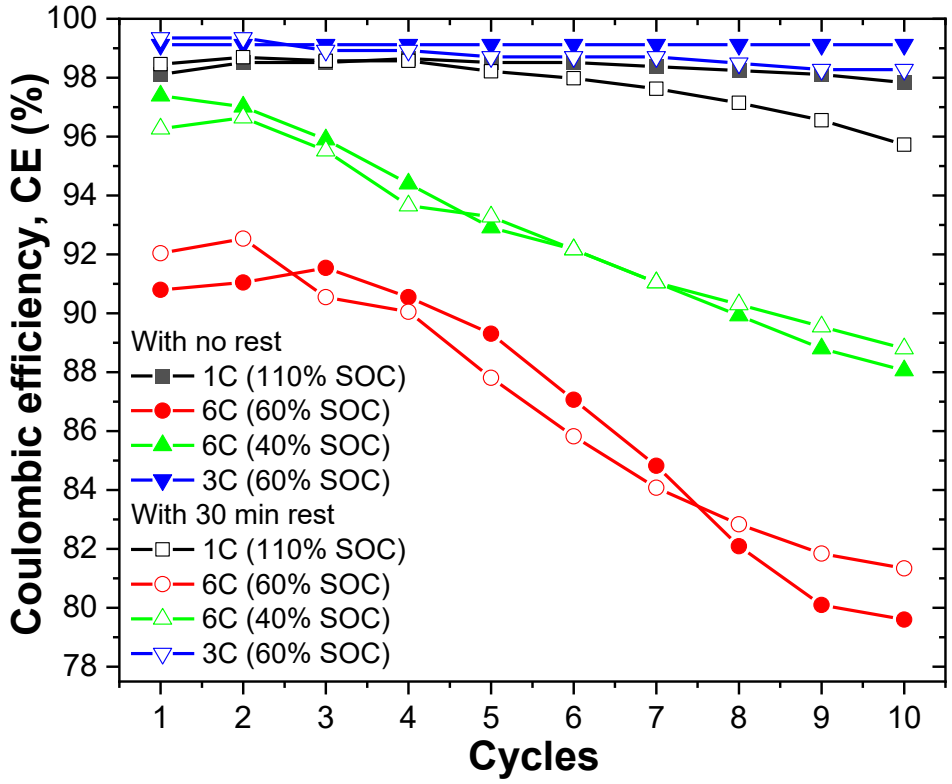

Figure S13. Comparison of average coulombic efficiency for Li/Gr half-cells at 1C charge 110% state of charge (SOC), 3C charge 60% SOC, 6C charge 60% SOC, and 40% SOC followed by C/5 discharge with rest and no rest conditions.